



**INSTITUTO POTOSINO DE INVESTIGACIÓN
CIENTÍFICA Y TECNOLÓGICA, A.C.**

POSGRADO EN CIENCIAS APLICADAS

A model-based controller for a three-phase four-wire shunt active filter

Tesis que presenta

Raymundo Enrique Torres Olguín

Para obtener el grado de

Maestro en Ciencias Aplicadas

En la opción de

Control y Sistemas Dinámicos

Director de la Tesis:

Dr. Gerardo Escobar Valderrama

San Luis Potosí, S.L.P., Septiembre de 2006



Constancia de aprobación de la tesis

La tesis (**A model-based controller for a three-phase four-wire shunt active filter**) presentada para obtener el Grado de de Maestro en Ciencias Aplicadas en la opción de Control y Sistemas Dinámicos fue elaborada por Raymundo Enrique Torres Olgún y aprobada el **1 de septiembre de 2006** por los suscritos, designados por el Colegio de Profesores de la División de Matemáticas Aplicadas y Sistemas Computacionales del Instituto Potosino de Investigación Científica y Tecnológica, A.C.

Dr. Gerardo Escobar Valderrama
(Director de la tesis)

Dr. Ciro Nuñez Gutierrez
(Sinodal)

Dr. Jorge Alberto Morales Saldaña
(Sinodal)

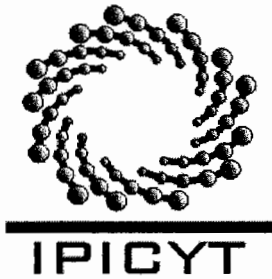
Dr. Daniel Melchor Aguilar
(Sinodal)



Créditos Institucionales

Esta tesis fue elaborada en la División de Matemáticas Aplicadas y Sistemas Computacionales del Instituto Potosino de Investigación Científica y Tecnológica, A.C., bajo la dirección del Dr. Gerardo Escobar Valderrama.

Durante la realización del trabajo el autor recibió una beca académica del Consejo Nacional de Ciencia y Tecnología (No. de registro 192566) y del Instituto Potosino de Investigación Científica y Tecnológica, A. C.



Instituto Potosino de Investigación Científica y Tecnológica, A.C.

Acta de Examen de Grado

COPIA CERTIFICADA

El Secretario Académico del Instituto Potosino de Investigación Científica y Tecnológica, A.C., certifica que en el Acta 011 del Libro Primero de Actas de Exámenes de Grado del Programa de Maestría en Ciencias Aplicadas en la opción de Control y Sistemas Dinámicos está asentado lo siguiente:

En la ciudad de San Luis Potosí a los 1 días del mes de septiembre del año 2006, se reunió a las 17:00 horas en las instalaciones del Instituto Potosino de Investigación Científica y Tecnológica, A.C., el Jurado integrado por:

Dr. Jorge Alberto Morales Saldaña	Presidente	UASLP
Dr. Gerardo Escobar Valderrama	Secretario	IPICYT
Dr. Ciro Alberto Núñez Gutiérrez	Sinodal externo	UASLP
Dr. Daniel Alejandro Melchor Aguilar	Sinodal	IPICYT

a fin de efectuar el examen, que para obtener el Grado de:

**MAESTRO EN CIENCIAS APLICADAS
EN LA OPCIÓN DE CONTROL Y SISTEMAS DINÁMICOS**

sustentó el C.

Raymundo Enrique Torres Olguín

sobre la Tesis intitulada:

A model-based controller for a three-phase four-wire shunt active filter

que se desarrolló bajo la dirección de


Dr. Gerardo Escobar Valderrama

El Jurado, después de deliberar, determinó

APROBARLO

Dándose por terminado el acto a las 18:40 horas, procediendo a la firma del Acta los integrantes del Jurado. Dando fé el Secretario Académico del Instituto.

A petición del interesado y para los fines que al mismo convengan, se extiende el presente documento en la ciudad de San Luis Potosí, S.L.P., México, a los 1 días del mes septiembre de 2006.


L.C.C. Ivonne Lizette Cuevas Velez
Jefa del Departamento de Asuntos Escolares


Dr. Marcia Bonilla Marín
Secretario Académico



Con todo mi amor a la persona que más me ha apoyado en estos dos años...Blanca

Agradecimientos

Primero me gustaría agradecer a mi asesor Gerardo Escobar cuyo apoyo técnico han permitido la realización de esta tesis, pero en especial por sus valiosos consejos más allá del plano académico, también agradezco al equipo del Laboratorio de Procesamiento y Calidad de la Energía Eléctrica: Andres, Hector, Juan Luis, Michael, Misael y Pánfilo que son un verdadero ejemplo de compañerismo. A mis profesores y amigos del departamento, Arturo Zavala, Daniel Melchor, David Lizárraga y Hugo Cabrera por sus innumerables lecciones.

Quiero agradecer especialmente a mi familia por apoyarme incondicionalmente en todo momento: mis padres(Francisca y Raymundo), mis hermanas (Marisol y Fátima), mis amigos más cercanos (Alejandro (tigre), Adbally, Calixto, Emeterio (Tello), Ivann, Javier (Fraga), Javier (Lepro), Jesús (Chuy), Juan Alejandro (Corpus), Juan Pablo, María Luisa, Mauro, Luis Carlos (Monroy), Ramiro y Victor) y por supuesto a mi novia Blanca González que me hace día a día mejor persona.

Raymundo E. Torres, San Luis Potosí, México Agosto del 2006

ABBREVIATIONS AND ACRONYMS

A/D	analog/digital
AC	alternating current
CE	chip enable
DC or dc	direct current
DSP	digital signal processor
IGBT	insolated gate bipolar transistor
LPF	low pass filter
LTI	linear time invariant
PF	power factor
PI	proportional plus integral
PWM	pulse width modulation
RMS	root mean square
THD	total harmonic distortion
TLSC	three leg split capacitor
VSI	voltage source inverter

RESUMEN

En los sistemas de distribución de energía eléctrica típicos es común encontrar cargas de tipo monofásico. Sin embargo estos sistemas son generalmente desbalanceados, debido a que la cargas son desigualmente distribuidas entre las fases, y distorsionados por la gran demanda de cargas de tipo no lineal. El desbalance y la distorsión produce efectos indeseables como son las componentes de secuencia negativa y cero. Por un lado, la secuencia negativa causa un excesivo calentamiento en máquinas eléctricas, saturación en transformadores y un indeseable rizo en los rectificadores [1], [2], [3], [4]. Y por el otro lado, la secuencia cero produce una excesiva pérdida y daño en el conductor neutro [3], [5]. Evidentemente, estos son efectos indeseables para los usuarios comerciales e industriales. Los filtros activos trifásicos han surgido como una solución exitosa a este tipo de problemas. Los filtros activos están diseñados para compensar potencia reactiva y distorsión armónica. Sin duda una de topologías más utilizadas es la de tres ramas con capacitor dividido para el inversor de fuente de voltaje, la cual puede aminorar las componentes de secuencia cero de la corriente (corriente homopolar). Sin embargo, se considera que hasta ahora no se ha presentado un modelo completo ni una clara explicación acerca de como la corriente homopolar es compensada.

En contraste con la mayoría de los controladores propuestos anteriormente, este trabajo presenta un controlador para un filtro activo paralelo trifásico de cuatro hilos basado en el modelo del sistema, el filtro tiene una topología de tres ramas de capacitor dividido para el inversor de fuente de voltaje. El controlador esta enfocado a compensar potencia reactiva y distorsión armónica en el caso general de corrientes de carga y voltaje de fuente distorsionados y desbalanceados. Además el control es capaz de compensar la componente homopolar de la corriente de carga debida principalmente a la distorsión generada por las cargas conectadas entre líneas y neutro.

En otras palabras, la corriente que fluye hacia la fuente por el neutro es considerablemente reducida sin modificar la topología. La clave para esta solución es el desarrollo de un modelo completo (en un esquema fijo) en términos de coordenadas $\alpha\beta\gamma$. Se le da una atención especial a la componente homopolar (componente γ) de la corriente de línea, el voltaje de línea y la entrada de control, la cual es muy importante en el diseño del controlador. Los resultados experimentales son probados en un prototipo de 2 KVA donde se muestran los beneficios de esta solución. Cabe mencionar que estos resultados fueron presentados en el “*IEEE Power Electronics Specialist Conference* ” en junio del 2006 [6].

ABSTRACT

It is well known that in a normal distribution systems a large amount of single-phase loads are connected. Therefore, distribution systems are inherently unbalanced and distorted due mainly to nonlinear loads unequally distributed between the phases. The unbalance and distortion produce undesired negative and zero sequence current components. On the one hand, the negative sequence causes excessive heating in machines, saturation of transformers and undesirable ripple in rectifiers [1], [2], [3], [4]. On the other hand, the zero sequence currents cause excessive power losses and even damage in the neutral line [3], [5]. Evidently, this is an undesirable or unacceptable situation for certain commercial and industrial users. Three phase active filters have emerged as a successful solution for such issues. They are designed to compensate reactive power and harmonic distortion. Perhaps the most appealing topology is the one based on three-leg split-capacitor (TLSC) voltage source inverter (VSI), which presumably compensates, in addition, the zero sequence (or homopolar) current component. However, to the best of our knowledge, there was not a complete model nor a clear comprehension about how the compensation process of the homopolar current component is performed.

In contrast with most of the controllers proposed so far, this work presents a model based controller for a three-phase four-wire shunt active filter, which uses a three-leg split-capacitor topology to implement the VSI. The controller is aimed to compensate reactive power and harmonic distortion in the general case of distorted and unbalanced source voltages and load currents. In addition, the controller is able to compensate for the homopolar component of the load current due mainly to distorting loads connected between a phase and the neutral line. In other words, the current flowing to the source via the neutral line can be considerably reduced and without modifying the actual topology.

Instrumental for our developments is the generation of a complete model in terms of (fixed frame) $\alpha\beta\gamma$ -coordinates. Special attention is given to the homopolar component (referred here also as the γ -component) of the line current, source voltage and control input, which are very important for the control design purpose. Experimental results in a 2 kVA prototype are provided to illustrate the benefits of our solution. This results was presented in the international congress PESC'06 [6].

CONTENTS

<i>Abbreviations and Acronyms</i>	xii
<i>Resumen</i>	xiv
<i>Abstract</i>	xvi
<i>1. Introduction</i>	1
<i>2. System description</i>	7
2.1 System model	7
2.1.1 Transformation to $\alpha\beta\gamma$ -coordinates	11
2.2 Control Objective	15
2.2.1 Current tracking	15
2.2.2 Homopolar current compensation	15
2.2.3 Capacitors voltage regulation	16
2.2.4 Capacitors voltage balance	16
2.3 Main Assumptions	16
<i>3. Controller design</i>	19

3.1	Introduction	19
3.2	Subsystem A	20
3.2.1	Inner control loop	20
3.2.2	Outer control loop	24
3.3	Subsystem B	27
3.3.1	Unperturbed System	29
3.3.2	Disturbance Rejection	29
4.	<i>Physical implementation</i>	35
4.1	Power stage	36
4.2	Control stage	41
4.3	Instrumentation stage	47
4.3.1	Source current sensor circuit	47
4.3.2	Input voltage sensor circuit	48
4.3.3	Capacitor voltage sensor circuit	49
4.3.4	Voltage limiter interface card	50
5.	<i>Results</i>	53
5.1	Introduction	53
5.2	Tracking results: harmonic disturbance and reactive power compensation	55
5.3	Homopolar current component compensation	61
5.4	Voltage regulation and voltage balance results	67

5.5 Transient Response	68
6. Conclusions	71

LIST OF TABLES

4.1	Technical details of the “Power Electronics Teaching System”.	37
4.2	Technical details of the variac 2510-3 type produced by Statco Energy Products TM	38
4.3	Technical details of the DS1103.	41
4.4	Devices and parameters of the control interface card.	43
4.5	Devices and parameters of the control interface card.	46
4.6	Devices and parameters used in the current sensor circuit.	49
4.7	Devices and parameters used in the input voltage sensor circuit.	49
4.8	Devices and parameters used in the capacitor voltage sensor circuit.	51
4.9	Devices and parameters used in the voltage limiter interface card.	52
5.1	The THD reached with the proposed controller in comparison with the THD of the load current.	57
5.2	Comparison of the percentage of the different harmonic components of the compensated neutral line current under the different control schemes.	66

LIST OF FIGURES

1.1	The generation, transmission and distribution stages in the power grid.	1
1.2	Three-phase four-wire system.	3
1.3	Third harmonic in a three phase four wire system.	3
1.4	(a) Three-leg split-capacitor, and (b) Four-leg full-bridge topologies.	5
2.1	Three-phase four-wire shunt active filter.	8
3.1	Block Diagram of the control (Subsystem A).	27
3.2	Block Diagram of the proposed controller.	33
4.1	Overall scheme of the three-phase four-wire shunt active filter showing the main stages	35
4.2	Picture of the prototype.	36
4.3	“Power Electronics Teaching System”.	37
4.4	Schematic of the distorted unbalanced load.	39
4.5	(Top plot) Three phase input voltages (x-axis 4 ms/div and y-axis 100 V/div), (four next plots, from top to bottom) the three load currents and the homopolar current (x-axis 4 ms/div and y-axis 5 A/div).	39

4.6	Frequency spectrum of (only one phase) (top) the source voltage and (bottom) the corresponding load current (x-axis 62.5 Hz/div and y-axis 10 dB/div).	40
4.7	(Top) Steady state time response of the load current homopolar component (x-axis 4 ms/div and y-axis 2 A/div), and (bottom) its frequency spectrum (x-axis 62.5 Hz/div and y-axis 10 dB/div).	40
4.8	Schematic of the different components of the dSPACE TM DS1103 card.	42
4.9	Picture of the control interface card.	43
4.10	Schematic of the control interface card.	44
4.11	Electric circuit for the relays used in the operational manoeuvres. . .	45
4.12	(a) Schematic of the current sensor and its signal conditioner, and (b) picture of the physical implementation.	48
4.13	(a) Electric circuit of the input voltage sensor, and (b) picture of the physical implementation.	50
4.14	(a) Schematic of the capacitor voltage sensor, and (b) picture of the physical implementation.	51
4.15	(a) Electric circuit of the voltage limiter, and (b) picture of the physical implementation.	52
5.1	(Top plot) Steady state responses of the active filter under the overall proposed solution. Three line voltage (250 V/div), (four last plots) three line current (10 A/div) and homopolar (neutral) current (5A/div).	56
5.2	(Top plot) Three line voltages (250 V/div), (four last plots) three load currents (10 A/div) and homopolar component of the load current (5A/div).	57

5.3	(Top) Spectra of line voltage v_{S3} (20 dB/div). (reference bottom plot) Spectra of line current i_{S3} (20 dB/div). (red bottom plot) Spectra of compensated line current i_{S3} (20 dB/div).	58
5.4	(From top to bottom) Steady state responses of the active filter under the conventional controller: line voltage (250 V/div), line current (10 A/div), load current (10 A/div) and (inverted) injected current (10 A/div).	59
5.5	(From top to bottom) Steady state responses of the active filter under the proposed controller with the homopolar compensation part disable: line voltage (250 V/div), line current (10 A/div), load current (10 A/div) and (inverted) injected current (10 A/div).	59
5.6	(From top to bottom) Steady state responses of the active filter under the overall proposed controller: line voltage (250 V/div), line current (10 A/div), load current (10 A/div) and (inverted) injected current (10 A/div).	60
5.7	Responses under the conventional controller (from top to bottom) : compensated neutral line current i_{S0} (5 A/div), homopolar component of the load current i_{L0} (5 A/div), and neutral injected current i_0 (5 A/div).	62
5.8	Responses under the proposed controller with the homopolar compensation part disabled (from top to bottom) : compensated neutral line current i_{S0} (5 A/div), homopolar component of the load current i_{L0} (5 A/div), and neutral injected current i_0 (5 A/div).	62
5.9	Responses under the overall proposed controller (from top to bottom) : compensated neutral line current i_{S0} (5 A/div), homopolar component of the load current i_{L0} (5 A/div), and neutral injected current i_0 (5 A/div).	63
5.10	(Top) Load current homopolar component i_{L0} (2 A/div) and (bottom) its frequency spectrum (10 dB/div).	63

-
- 5.11 **(Top)** Compensated neutral line current i_{S0} (2 A/div) and **(bottom)** its frequency spectrum (10 dB/div) with conventional controller. 64
- 5.12 **(Top)** Compensated neutral line current i_{S0} (2 A/div) and **(bottom)** its frequency spectrum (10 dB/div) with the proposed controller disabling the homopolar compensation part. 64
- 5.13 **(Top)** Compensated neutral line current i_{S0} (2 A/div) and **(bottom)** its frequency spectrum (10 dB/div) with the overall proposed controller. 65
- 5.14 **(From top to bottom)** Sum of the capacitor voltages x_4 (50 V/div), difference of the capacitor voltages x_5 (50 V/div), and scaled apparent conductance $gv_{S,RMS}^2$ (500 W/div). 67
- 5.15 Transient responses of the active filter under a load change from 350 Ω to 175 Ω **(rom top to bottom)**: line voltage (100 V/div), compensated neutral line current i_{S0} (2 A/div), homopolar component of the load current i_{L0} (2 A/div), and injected neutral current i_0 (2 A/div). 68
- 5.16 Transient responses of the active filter under a load change from 175 Ω to 350 Ω **(from top to bottom)**: line voltage (100 V/div), compensated neutral line current i_{S0} (2 A/div), homopolar component of the load current i_{L0} (2 A/div), and injected neutral current i_0 (2 A/div). 69

1. INTRODUCTION

A utility company is aimed to generate, transmit and distribute a voltage signal, typically three-phase alternating current (AC). The conjunction of all these stages in the process conform a power system as the one shown in Fig. 1.1. Roughly speaking, the main objective of the utility company is to produce sinusoidal voltage signals, one per phase, with a fairly constant amplitude and at a given fixed frequency (50 or 60 Hz). These voltage signals are delivered to the final users in the power grid system. However, this objective is not easy to accomplish due mainly to the existence of distorting loads. These loads, also referred as nonlinear loads, produce periodic non sinusoidal currents composed of higher harmonics multiples of the fundamental frequency (50 or 60 Hz). These distorted currents, also referred as harmonic currents, represent a pollution to the electrical grid, and entail a series of issues such as distorted voltages, which can adversely impact the system performance in different ways.

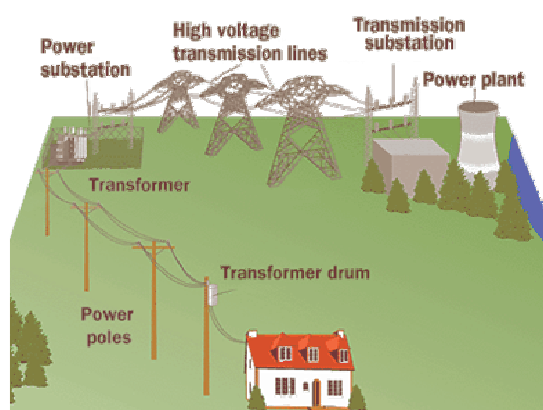


Figure 1.1 The generation, transmission and distribution stages in the power grid.

The most typical connection in a distribution system is a three-phase delta-wye system as the one shown in Fig. 1.2. Three-phase delta-delta systems are limited to motor and heavy machinery loads. It is well known that most commercial and industrial facilities use three phase power, where a large portion of them are wye connected, as previously mentioned. Of special concern are the single-phase loads equipped with rectifier front-end power supplies, e.g., electronic lighting ballasts, appliances, personal computers, etc. When these loads are connected line to neutral in a three phase wye-connected system, the returning current in the neutral conductor can reach surprising levels, even in the load balanced condition. The combined current of the three phases returning through the neutral wire is also known as homopolar current. Traditionally, it is considered that if the loads on each phase are balanced, then the return currents in the neutral wire will cancel each other and thus, the neutral current will be zero. This, however, is not longer valid in case of distorting loads, where as previously mentioned, currents can combine to produce a considerable neutral current. And contrary to traditional thinking, efforts made to balance loads on the three phases subject to high current distortion conditions, may even contribute to increase the neutral current [7]. Moreover, as it will be shown in this work, the traditional techniques aimed to compensate for harmonic distortion, also contribute to increase the neutral current. Typical unfiltered single phase electronic loads produce a large amount of 3rd harmonic, plus decreasing percentages of all higher order odd harmonics. Of those harmonics, only the triplen harmonics (evenly divisible by 3), i.e., 3th, 9th, 15th, etc. contribute to the neutral problem.

The generation of the neutral current from a distorting balanced load can be easily explained from Fig. 1.3 [7]. Consider that the current waveform is typically so narrow as to be “non-overlapping” on all three phases. This means that only one phase of the three phase system carries current at any instant of time. Under these circumstances, the only return path for each current is the neutral conductor. As a result, the number of current pulses accumulated in the panel neutral is three times that in the lines. The root mean square (RMS) current increase, from one to three current pulses in a common time interval, which represents a 173%.

Excessive homopolar current entails several negative effects which are summarized here:

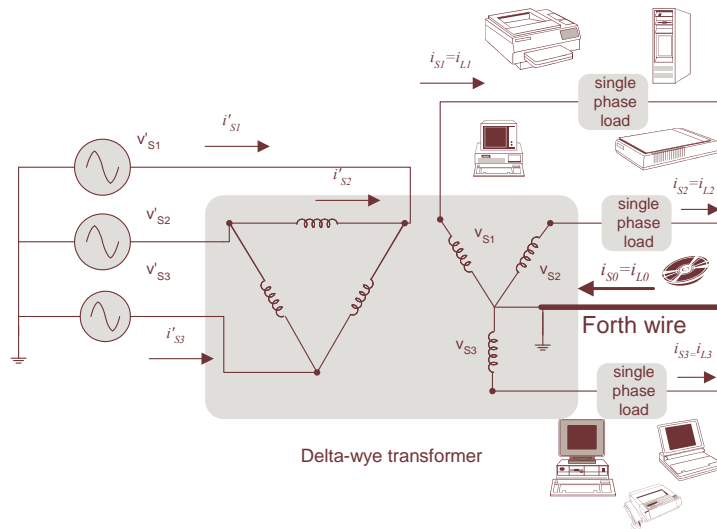


Figure 1.2 Three-phase four-wire system.

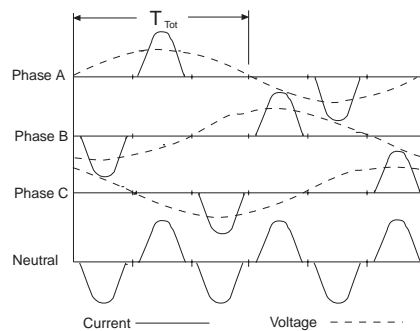


Figure 1.3 Third harmonic in a three phase four wire system.

- ▷ Excessive stress due to heating on transformers.
- ▷ Insulation breakdown on transformers.
- ▷ Lower operating efficiency and short life span on transformers.
- ▷ Acoustic noise on transformers.
- ▷ Overheating and damage of neutral conductor.
- ▷ Common noise voltage.

To explain this problems, notice that the neutral current flows through the neutral conductor to the three-phase transformer. It passes through the wye secondary, and is coupled into the delta primary. The transformer theory shows that balanced triplen harmonic currents can not pass out of a delta winding. Instead, they are circulated within the winding and dissipated as heat. In other words, the primary of the transformer is now carrying not only the phase current needed to the supply secondary loads, but also the circulating homopolar currents. Thus, a transformer that should, according to the loads being served, be lightly loaded, can actually be reaching overload. These high currents are responsible for the transformer heating and breaker tripping problems [8].

The active filters for three phase systems have been successfully developed to compensate reactive power, unbalance and harmonic distortion, in the general case of distorted and unbalanced source voltages and load currents, for the three-phase three-wire systems. To somehow provide a solution for the homopolar problem different modifications to the conventional topology have emerged ([9], [2] and [5]). Of those modifications, perhaps the most known are the three-leg split-capacitor (TLSC) and the four-leg topologies shown in Fig. 1.4.

The TLSC topology shown in Fig. 1.4(a) is the most popular one because of its lower number of power semiconductor devices [10] [11]. However, this topology has some disadvantages mostly related with the dc capacitor voltage balance control, which explains the oversize of capacitors. Several control strategies have been reported for the split-capacitor topology like the dynamic hysteresis current control proposed by [12] [13], space-vector-based current controlled in $\alpha\beta\gamma$ coordinates proposed in [14], the neural network technologies proposed in [15] or the strategies of instantaneous power compensation proposed in [16].

The four-leg topology shown in Fig. 1.4(b) was proposed with the aim to increase the controllability at the expense of increasing the semiconductor devices, in contrast to the split-capacitor topology. As expected, the modulation techniques are more complex, and the computational load is also increased. Several solutions based on three dimensional space vector modulation are proposed in [17], [18], [19]. An interesting current hysteresis controller is also proposed in [20].

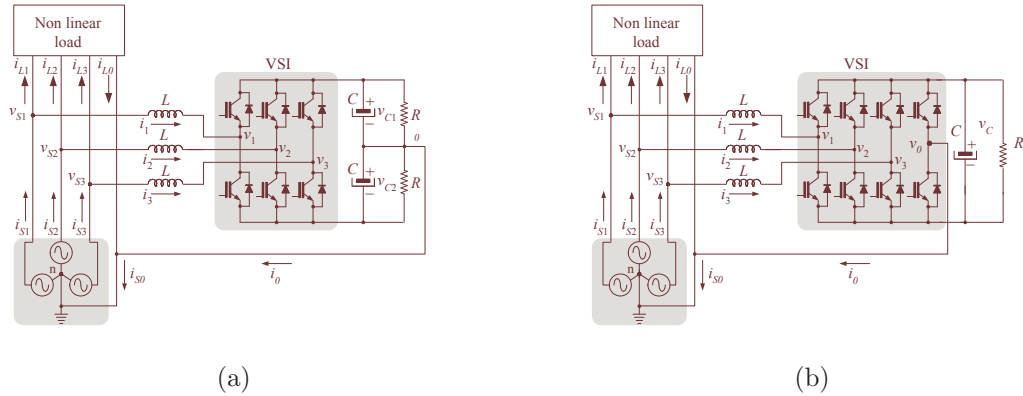


Figure 1.4 (a) Three-leg split-capacitor, and (b) Four-leg full-bridge topologies.

Although three-phase four-wire active filters were introduced in the 1980's [9] [12], it has been observed that due to the richness of control paradigms encountered when considering the neutral connection, still several efforts are carried out to better understand and control such systems.

This work presents a control solution for a three-phase four-wire shunt active filter, which uses the TLSC topology. The design of the proposed controller is based on the model of this topology. The controller is aimed to reduce the homopolar current flowing in the line neutral wire, and simultaneously, to balance the voltage of both dc side capacitors. Additionally the controller can compensate the reactive power and harmonic distortion produced in the general case of distorted and unbalance source voltage and load current. Instrumental in the developments is the consideration of the special attention is given to the γ component of the line current, source voltage and control input, which were instrumental for the control design purpose. This controller neither require a topology modification nor a complex modulation algorithm. In fact, the only modification is at the level of control, whose structure is very close to that of the conventional, except that it includes additional terms to finally accomplish the complete objective with a formal justification. This perhaps represents one of the main advantages of this work respect to other solutions. Finally, the proposed control scheme has been implemented and tested in a 2 KVA prototype of a three-phase four-wire shunt active filter and the experimental results are presented.

This thesis report is organized as follows: In Chapter 2 the system description is established. In particular, the system configuration, the mathematical model and the control objective are explained. Chapter 3 presents, in a detailed form, the design of the proposed controller. Chapter 4 describes the physical implementation of all stages that conform the prototype of the three-phase four-wire active filter. In Chapter 5, the experimental results are shown. Finally, Chapter 6 gives some concluding remarks.

2. SYSTEM DESCRIPTION

2.1 System model

The three-phase four-wire shunt active filter studied in this thesis is depicted in Fig. 2.1. This system is composed of a TLSC voltage source inverter (VSI). The VSI is branched to the line via inductors of value L . Two capacitors C in series are connected on the dc-side. The point of connection between the two capacitors, also referred as the neutral point, is connected to the fourth wire, which is also referred indistinctly as neutral wire. This system array is working as a *distribution static compensator* (D-Statcom) which is mainly designed to compensate reactive power, unbalance and harmonic distortion in the line current due to a distorted load current. In addition, the neutral point is connected to the fourth-wire to allow compensation of the homopolar component of the load current. Switching and other losses are lumped and modeled as unknown constant resistive elements R . In fact the same C and R have been considered for both capacitors.

The system parameters and variable are described next:

$i_{Sk}(t)$	currents in the source line $\forall k \in \{1, 2, 3, 0\}$;
$i_{Lk}(t)$	current produced by the load $\forall k \in \{1, 2, 3, 0\}$;
$i_k(t)$	compensating currents $\forall k \in \{1, 2, 3, 0\}$;
$v_{Sk}(t)$	source voltages (referred to the neutral point “n”) $\forall k \in \{1, 2, 3, 0\}$;
$v_{Ck}(t)$	capacitors voltages $\forall k \in \{1, 2\}$;
$v_k(t)$	voltages at the input of the VSI (referred to “n”) $\forall k \in \{1, 2, 3\}$;
L	filter inductance;
C	dc side (output) capacitance;
R	resistive element due to losses.

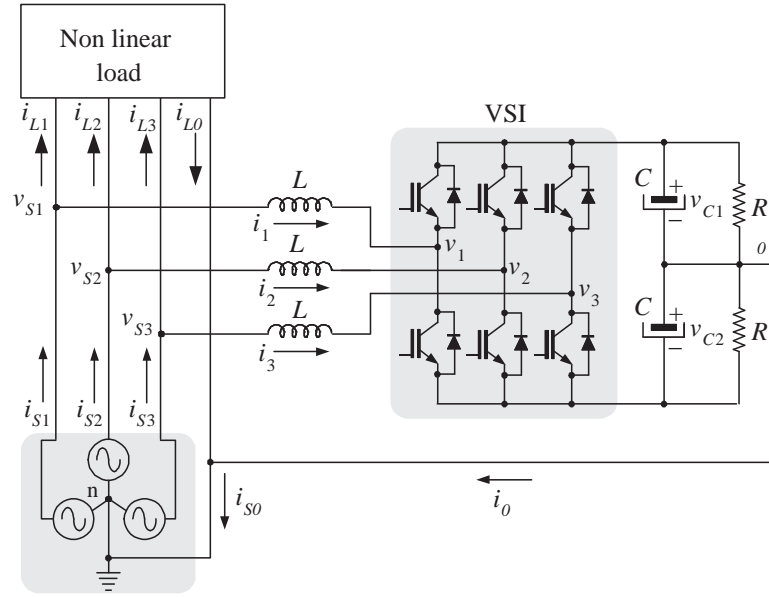


Figure 2.1 Three-phase four-wire shunt active filter.

The modeling process is supported by Kirckoff's laws and is obtained as follows. First, the dynamics of the inductor currents is obtained from direct application of the Kirchhoff's Voltage Law (KVL). This gives the following set of equations

$$v_{S1}(t) = L \frac{d}{dt} i_1(t) + v_1(t) \quad (2.1)$$

$$v_{S2}(t) = L \frac{d}{dt} i_2(t) + v_2(t) \quad (2.2)$$

$$v_{S3}(t) = L \frac{d}{dt} i_3(t) + v_3(t) \quad (2.3)$$

The switch positions vector is defined as $\boldsymbol{\delta}(t) = [\delta_1(t), \delta_2(t), \delta_3(t)]^\top$ where each component $\delta_k(t) (\forall k \in \{1, 2, 3\})$ takes values in the discrete set $\{0, 1\}$. In this case "0" means that the switch is "off" while "1" means that the switch is "on". The complement is given by $\bar{\delta}_k(t) = 1 - \delta_k(t) (\forall k \in \{1, 2, 3\})$. From now on, the time argument in all variables is eliminated to reduce the notation. Moreover, notations $\frac{d}{dt}(\cdot)$, $\frac{d(\cdot)}{dt}$ and $(\dot{\cdot})$ are used indistinctly to represent the time derivative of (\cdot) . Also, the matrices and vectors are highlighted with boldface characters to distinguish them

from the scalar variables.

Notice that, if $\delta_k = 1$ ($\bar{\delta}_k = 0$) then $v_k = v_{C1}$, while $v_k = -v_{C2}$ for $\delta_k = 0$ ($\bar{\delta}_k = 1$) $\forall k \in \{1, 2, 3\}$. The voltage at the input of the VSI is given by

$$v_k = -(1 - \delta_k)v_{C2} + \delta_k v_{C1} \quad (2.4)$$

Direct substitution of equation (2.4) in (2.1), (2.2) and (2.3) yields

$$v_{S1} = L \frac{d}{dt} i_1 - (1 - \delta_1)v_{C2} + \delta_1 v_{C1}$$

$$v_{S2} = L \frac{d}{dt} i_2 - (1 - \delta_2)v_{C2} + \delta_2 v_{C1}$$

$$v_{S3} = L \frac{d}{dt} i_3 - (1 - \delta_3)v_{C2} + \delta_3 v_{C1}$$

which in matrix notation can be rewritten as

$$\mathbf{v}_S = L \frac{d}{dt} \mathbf{i} - v_{C2} \begin{pmatrix} 1 \\ 1 \\ 1 \end{pmatrix} + (v_{C1} + v_{C2}) \boldsymbol{\delta} \quad (2.5)$$

where $\mathbf{v}_S = [v_{S1}, v_{S2}, v_{S3}]^\top$ is the vector of source voltages referred to “n”, $\mathbf{i} = [i_1, i_2, i_3]^\top$ is the vector of compensating currents and $\boldsymbol{\delta} = [\delta_1, \delta_2, \delta_3]^\top$ is the vector of switch positions.

Application of Kirchhoff’s current law (KCL) yields the following expressions representing the dynamics of the capacitors voltages

$$i_{C1} = \delta_1 i_1 + \delta_2 i_2 + \delta_3 i_3 - \frac{v_{C1}}{R} \quad (2.6)$$

$$\begin{aligned} i_{C2} &= \bar{\delta}_1 i_1 + \bar{\delta}_2 i_2 + \bar{\delta}_3 i_3 - \frac{v_{C2}}{R} \\ &= -(1 - \delta_1) i_1 - (1 - \delta_2) i_2 - (1 - \delta_3) i_3 - \frac{v_{C2}}{R} \\ &= -i_0 + \delta_1 i_1 + \delta_2 i_2 + \delta_3 i_3 - \frac{v_{C2}}{R} \end{aligned} \quad (2.7)$$

where $i_0 = i_1 + i_2 + i_3$ has been used.

Summarizing, the complete dynamics of the three-phase four-wire shunt active

filter is given by

$$L \frac{d\mathbf{i}}{dt} = \mathbf{v}_S + v_{C2} \begin{pmatrix} 1 \\ 1 \\ 1 \end{pmatrix} - (v_{C1} + v_{C2}) \boldsymbol{\delta} \quad (2.8)$$

$$C\dot{v}_{C1} = \boldsymbol{\delta}^\top \mathbf{i} - \frac{v_{C1}}{R} \quad (2.9)$$

$$C\dot{v}_{C2} = -i_0 + \boldsymbol{\delta}^\top \mathbf{i} - \frac{v_{C2}}{R} \quad (2.10)$$

where the relationships $i_{C1} = C\dot{v}_{C1}$ and $i_{C2} = C\dot{v}_{C2}$ have been used.

The model composed by (2.8)-(2.10) belongs to the class of hybrid systems, where the control, represented by vector $\boldsymbol{\delta}$, takes values in a discrete set. However, the control design in hybrid systems is much more involved than in continuous systems. Therefore, in the present work it is assumed that the switching sequences are implemented by means of a pulse width modulation (PWM) scheme switching at a relatively high frequency (this is a common practice among most practitioners). Hence, the control problem is reduced to design the vector of duty ratios to feed such a PWM block. Based on these considerations, the vector of switch positions $\boldsymbol{\delta}$, where each entry takes values in the discrete set $\{0, 1\}$, is replaced by the vector of duty ratios, where each entry takes values in the continuous range $[0, 1]$. To avoid an extra definition, the same variable $\boldsymbol{\delta}$ is used to represent either the vector of switch positions or the vector of duty ratios.

To facilitate the notation, it is convenient to consider the following transformation

$$\delta_k = \frac{u_k + 1}{2}, \quad \forall k \in \{1, 2, 3\} \quad (2.11)$$

Notice that, if $\delta_k \in [0, 1]$ then $u_k \in [-1, 1]$.

Under the above consideration (2.4) can be rewritten as follows

$$\begin{aligned} v_k &= \left(\frac{1 + u_k}{2} \right) v_{C1} - \left(\frac{1 - u_k}{2} \right) v_{C2} \\ &= \frac{1}{2}(v_{C1} - v_{C2}) + \frac{1}{2}(v_{C1} + v_{C2})u_k, \quad \forall k \in \{1, 2, 3\} \end{aligned} \quad (2.12)$$

Direct substitution of (2.11) in (2.8) yields

$$L \frac{d}{dt} \mathbf{i} = \mathbf{v}_S - \frac{1}{2}(v_{C1} - v_{C2}) \begin{pmatrix} 1 \\ 1 \\ 1 \end{pmatrix} - \frac{1}{2}(v_{C1} + v_{C2}) \mathbf{u} \quad (2.13)$$

The control input vector is now defined as $\mathbf{u} \triangleq [u_1, u_2, u_3]^\top$.

Using (2.11) in (2.9)-(2.10) yields

$$\begin{aligned} C\dot{v}_{C1} &= \left(\frac{u_1 + 1}{2}\right) i_1 + \left(\frac{u_2 + 1}{2}\right) i_2 + \left(\frac{u_3 + 1}{2}\right) i_3 - \frac{v_{C1}}{R} \\ C\dot{v}_{C2} &= \left(\frac{u_1 + 1}{2}\right) i_1 + \left(\frac{u_2 + 1}{2}\right) i_2 + \left(\frac{u_k + 1}{2}\right) i_3 - \frac{v_{C2}}{R} - i_0 \end{aligned}$$

The above equation can also be expressed as

$$C\dot{v}_{C1} = \frac{\mathbf{u}^\top \mathbf{i}}{2} + \frac{1}{2} i_0 - \frac{v_{C1}}{R} \quad (2.14)$$

$$C\dot{v}_{C2} = \frac{\mathbf{u}^\top \mathbf{i}}{2} - \frac{1}{2} i_0 - \frac{v_{C2}}{R} \quad (2.15)$$

where $i_0 = i_1 + i_2 + i_3$ has been used again.

Summarizing, the complete dynamics of the three-phase four-wire shunt active filter is given by

$$L \frac{d}{dt} \mathbf{i} = \mathbf{v}_S - \frac{1}{2}(v_{C1} - v_{C2}) \begin{pmatrix} 1 \\ 1 \\ 1 \end{pmatrix} - \frac{1}{2}(v_{C1} + v_{C2}) \mathbf{u} \quad (2.16)$$

$$C\dot{v}_{C1} = \frac{\mathbf{u}^\top \mathbf{i}}{2} + \frac{1}{2} i_0 - \frac{v_{C1}}{R} \quad (2.17)$$

$$C\dot{v}_{C2} = \frac{\mathbf{u}^\top \mathbf{i}}{2} - \frac{1}{2} i_0 - \frac{v_{C2}}{R} \quad (2.18)$$

2.1.1 Transformation to $\alpha\beta\gamma$ -coordinates

For the control design purpose, it is very convenient to express the resulting model represented by (2.16)-(2.18) in terms of the (fixed frame) $\alpha\beta\gamma$ -coordinates. For this, the conventional complete Clark transformation (see [21]) is used as follows.

$$\mathbf{x}_{\alpha\beta\gamma} = \mathbf{T} \mathbf{x}_{abc} \quad , \quad \mathbf{x}_{abc} = \mathbf{T}^{-1} \mathbf{x}_{\alpha\beta\gamma}$$

where $\mathbf{x}_{abc} \in \mathbb{R}_3$ represents any vector in the original coordinates and $\mathbf{x}_{\alpha\beta\gamma}$ its representation in terms of $\alpha\beta\gamma$ -coordinates. The transformation matrix used is given by

$$\mathbf{T} = \sqrt{\frac{2}{3}} \begin{pmatrix} 1 & -\frac{1}{2} & -\frac{1}{2} \\ 0 & \frac{\sqrt{3}}{2} & -\frac{\sqrt{3}}{2} \\ \frac{1}{\sqrt{2}} & \frac{1}{\sqrt{2}} & \frac{1}{\sqrt{2}} \end{pmatrix}$$

with the following property $\mathbf{T}^{-1} = \mathbf{T}^\top$. Notice that, the coordinate γ corresponds to the homopolar or zero component of the three phase signals. This component is usually neglected, most of all in the three-wire cases, however, as will be shown later, it is of special interest for the analysis and compensation of the homopolar component of signals in the fourth-wire case.

Direct application of the Clark's transformation to the inductor currents dynamics (2.16) yields

$$L \frac{d}{dt} \mathbf{i}_{\alpha\beta\gamma} = \mathbf{v}_{S\alpha\beta\gamma} - \frac{\sqrt{3}}{2} (v_{C1} - v_{C2}) \begin{pmatrix} 0 \\ 0 \\ 1 \end{pmatrix} - \frac{1}{2} (v_{C1} + v_{C2}) \mathbf{u}_{\alpha\beta\gamma} \quad (2.19)$$

For the control design purpose, it is convenient to split subsystem (2.19) in the following two subsystems

$$L \frac{d}{dt} \mathbf{i}_{\alpha\beta} = \mathbf{v}_{S\alpha\beta} - \frac{1}{2} (v_{C1} + v_{C2}) \mathbf{u}_{\alpha\beta} \quad (2.20)$$

$$L \frac{d}{dt} i_\gamma = \mathbf{v}_{S\gamma} - \frac{\sqrt{3}}{2} (v_{C1} - v_{C2}) - \frac{1}{2} (v_{C1} + v_{C2}) \mathbf{u}_\gamma \quad (2.21)$$

Now, applying the Clark's transformation to the capacitor voltages dynamics yields

$$\begin{aligned} C \dot{v}_{C1} &= \frac{1}{2} (\mathbf{T}^{-1} \mathbf{u}_{\alpha\beta\gamma})^\top \mathbf{T}^{-1} \mathbf{i}_{\alpha\beta\gamma} + \frac{1}{2} i_0 - \frac{v_{C1}}{R} \\ &= \frac{1}{2} \mathbf{u}_{\alpha\beta\gamma}^\top \mathbf{i}_{\alpha\beta\gamma} + \frac{\sqrt{3}}{2} i_\gamma - \frac{v_{C1}}{R} \end{aligned}$$

where $i_\gamma = \sqrt{\frac{2}{3}} \left(\frac{i_1}{\sqrt{2}} + \frac{i_2}{\sqrt{2}} + \frac{i_3}{\sqrt{2}} \right) = \frac{1}{\sqrt{3}} i_0$.

In the similar way

$$C \dot{v}_{C2} = \frac{1}{2} \mathbf{u}_{\alpha\beta\gamma}^\top \mathbf{i}_{\alpha\beta\gamma} - \frac{\sqrt{3}}{2} i_\gamma - \frac{v_{C2}}{R}$$

The following definitions are considered to further reduce the notation. Notice that, they correspond to the sum and the difference between the capacitors voltages, which are natural variables for the system description. This description is very useful in the control design, as will be shown later.

$$x_4 \triangleq v_{C1} + v_{C2} \quad , \quad x_5 \triangleq v_{C1} - v_{C2}$$

The dynamics of the sum and the difference of capacitor voltages, according to the definitions above, are given by

$$C\dot{x}_4 = \mathbf{u}_{\alpha\beta\gamma}^\top \mathbf{i}_{\alpha\beta\gamma} - \frac{x_4}{R} \quad (2.22)$$

$$C\dot{x}_5 = \sqrt{3}i_\gamma - \frac{x_5}{R} \quad (2.23)$$

Moreover, with the idea of reducing the number of current sensors, it is proposed to describe the system in terms of the source currents $\mathbf{i}_{S\alpha\beta\gamma}$ instead of the inductor currents $\mathbf{i}_{\alpha\beta\gamma}$. For this purpose, the following relationship is considered

$$\mathbf{i}_{S\alpha\beta\gamma} = \mathbf{i}_{L\alpha\beta\gamma} + \mathbf{i}_{\alpha\beta\gamma} \quad (2.24)$$

which corresponds to the Clarke's transformation of $\mathbf{i}_S = \mathbf{i}_L + \mathbf{i}$.

Direct substitution of (2.24) in (2.20)-(2.21) and (2.22)-(2.23) yields

$$\begin{aligned} L \frac{d}{dt} \mathbf{i}_{S\alpha\beta} &= \mathbf{v}_{S\alpha\beta} - \frac{1}{2}(x_4) \mathbf{u}_{\alpha\beta} + L \frac{d}{dt} \mathbf{i}_{L\alpha\beta} \\ L \frac{d}{dt} i_{S\gamma} &= v_{S\gamma} - \frac{\sqrt{3}}{2}(x_5) - \frac{1}{2}x_4 u_\gamma + L \frac{d}{dt} i_{L\gamma} \\ C\dot{x}_4 &= \mathbf{u}_{\alpha\beta\gamma}^\top (\mathbf{i}_{S\alpha\beta\gamma} - \mathbf{i}_{L\alpha\beta\gamma}) - \frac{x_4}{R} \\ C\dot{x}_5 &= \sqrt{3}(i_{S\gamma} - i_{L\gamma}) - \frac{x_5}{R} \end{aligned}$$

The model expressions can be further reduced by proposing the following change of variables

$$\boldsymbol{\epsilon}_{\alpha\beta\gamma} \triangleq \frac{x_4 \mathbf{u}_{\alpha\beta\gamma}}{2} \quad , \quad z_4 \triangleq \frac{x_4^2}{2}$$

Summarizing, after all the proposed change of variables, the complete model ex-

pressed in terms of $\alpha\beta\gamma$ -coordinates is given by

$$L \frac{d}{dt} \mathbf{i}_{S\alpha\beta} = \mathbf{v}_{S\alpha\beta} - \boldsymbol{\varepsilon}_{\alpha\beta} + L \frac{d}{dt} \mathbf{i}_{L\alpha\beta} \quad (2.25)$$

$$L \frac{d}{dt} i_{S\gamma} = v_{S\gamma} - \frac{\sqrt{3}}{2} x_5 - \varepsilon_\gamma + L \frac{d}{dt} i_{L\gamma} \quad (2.26)$$

$$C \dot{z}_4 = 2\boldsymbol{\varepsilon}_{\alpha\beta\gamma}^\top (\mathbf{i}_{S\alpha\beta\gamma} - \mathbf{i}_{L\alpha\beta\gamma}) - \frac{2z_4}{R} \quad (2.27)$$

$$C \dot{x}_5 = \sqrt{3} (i_{S\gamma} - i_{L\gamma}) - \frac{x_5}{R} \quad (2.28)$$

where $\boldsymbol{\varepsilon}_{\alpha\beta\gamma}$ has been split in

$$\boldsymbol{\varepsilon}_{\alpha\beta} \triangleq \frac{x_4 \mathbf{u}_{\alpha\beta}}{2}, \quad \varepsilon_\gamma \triangleq \frac{x_4 u_\gamma}{2}$$

Notice that, equation (2.25) and (2.27) have been decoupled from (2.26) and (2.28). This allows to split the overall system in the following two subsystems.

Subsystem A

$$L \frac{d}{dt} \mathbf{i}_{S\alpha\beta} = \mathbf{v}_{S\alpha\beta} - \boldsymbol{\varepsilon}_{\alpha\beta} + L \frac{d}{dt} \mathbf{i}_{L\alpha\beta} \quad (2.29)$$

$$C \dot{z}_4 = 2\boldsymbol{\varepsilon}_{\alpha\beta}^\top (\mathbf{i}_{S\alpha\beta} - \mathbf{i}_{L\alpha\beta}) - \frac{2z_4}{R} + 2\varepsilon_\gamma (i_{S\gamma} - i_{L\gamma}) \quad (2.30)$$

Subsystem B

$$L \frac{d}{dt} i_{S\gamma} = v_{S\gamma} - \frac{\sqrt{3}}{2} (x_5) - \varepsilon_\gamma + L \frac{d}{dt} i_{L\gamma} \quad (2.31)$$

$$C \dot{x}_5 = \sqrt{3} (i_{S\gamma} - i_{L\gamma}) - \frac{x_5}{R} \quad (2.32)$$

On the one hand, Subsystem A coincides with the model of the conventional three-phase three-wire shunt active filter, except for the disturbance signal $2\varepsilon_\gamma (i_{S\gamma} - i_{L\gamma})$ on the right hand side of (2.30). As expected, the current dynamics is strongly connected with the regulation of the capacitors voltages sum. On the other hand, Subsystem B describes the extra dynamics, which is due to the existence of the fourth wire connection on the system. Notice that, the current that flows on the fourth wire is strongly related with the difference of the capacitors voltages. As both subsystems are decoupled from one another, they can be treated separately, thus facilitating the control design, as shown later.

2.2 Control Objective

As in the conventional control for a three-phase three-wire system, a tracking and a regulation objectives are established in Subsystem A. Then, for Subsystem B, two additional objectives arise. First, to reduce the current (homopolar component) flowing through the fourth wire, and second, to maintain the capacitors voltages difference as close as possible to zero (in the average) to guarantee the capacitors voltage balance.

2.2.1 Current tracking

This objective consists in forcing the source current to track a reference proportional to the source voltage only in the α and β components. In this way, the source perceives the connection of both load and active filter as a simple resistance, thus guaranteeing a power factor (PF) close to one. The last with the additional advantages of low cost transmission, energy quality improvement, stability, and so on. For the fulfillment of this objective, the active filter should be able to inject the necessary current to cancel the distortion caused by the load current. Mathematically, this objective can be expressed as

$$\mathbf{i}_{S\alpha\beta} \rightarrow \mathbf{i}_{S\alpha\beta}^* = g\mathbf{v}_{S\alpha\beta} \quad (2.33)$$

where g is a scalar, yet to be determined, that represents the scaled apparent conductance observed by the voltage source.

2.2.2 Homopolar current compensation

One of the main contributions of this work is the introduction of a compensation scheme to eliminate the homopolar component of the source current vector, that is, to cancel the current flowing through the fourth wire (neutral line). The current in the neutral line is related with overheating and damage of the neutral conductors, as well as the origin of higher common mode voltage, and so on. This objective can be expressed formally as follows

$$i_{S\gamma} \rightarrow i_{S\gamma}^* = 0 \quad (2.34)$$

2.2.3 Capacitors voltage regulation

For the correct operation of the active filter, the sum of both capacitors voltages is forced to maintain a constant value. This guarantees that enough energy is stored in the capacitors for the correct accomplishment of the previous objectives. This objective can be expressed as follows

$$x_4 \rightarrow x_4^* = 2V_d \quad , \quad z_4 \rightarrow z_4^* = 2v_d^2 \quad (2.35)$$

where V_d is the reference constant value for each capacitor voltage.

2.2.4 Capacitors voltage balance

It is also necessary to guarantee that the difference between both capacitors voltages approaches zero (in the average). The fulfillment of this objective, and the above capacitors voltage regulation objective is necessary and sufficient to guarantee that both capacitors reach the same voltage value (in average). This has the additional advantages of producing symmetrical patterns in the VSI generated voltage and a safe operation. Mathematically, this objective can be expressed as

$$x_5 \rightarrow x_5^* = 0 \quad (2.36)$$

2.3 Main Assumptions

- A1. For the control design purpose, the parameters L , C and R are all assumed to be unknown constants, however the nominal values of these parameters are necessary to tune the control parameter. In other words, although these parameters do not appear explicitly in the controller expressions, it is required to know their nominal values for a first controller parameters tuning. A robustness study with respect to parameters variations would be of a great interest, but it is out of the scope of the present work.
- A2. The fundamental frequency ω_0 is consider a known constant.

- A3. A sufficiently high frequency is assumed to implement the switching control sequence (using for instance a PWM scheme). After this assumption, as mentioned before, the vector of switch positions $\boldsymbol{\delta}$ can be replaced by the vector of corresponding duty ratios which are continuous signals, thus facilitating enormously the control design.
- A4. The load current $\mathbf{i}_{L\alpha\beta}$ and source voltage $\mathbf{v}_{S\alpha\beta}$ are assumed to be (independently) unbalanced periodic signals that contain mainly odd harmonics of the fundamental frequency ω_0 . Therefore, these signals can be expressed in the form of Fourier series as follows

$$\mathbf{v}_{S\alpha\beta} = \sum_{k \in \mathcal{H}} (\mathbf{e}^{\mathbf{J}k\omega_0 t} V_{s,k}^p + \mathbf{e}^{-\mathbf{J}k\omega_0 t} V_{s,k}^n) \quad (2.37)$$

$$\mathbf{i}_{L\alpha\beta} = \sum_{k \in \mathcal{H}} (\mathbf{e}^{\mathbf{J}k\omega_0 t} I_{L,k}^p + \mathbf{e}^{-\mathbf{J}k\omega_0 t} I_{L,k}^n) \quad (2.38)$$

$$\mathbf{e}^{\mathbf{J}\omega_0 kt} = \begin{pmatrix} \cos(\omega_0 kt) & -\sin(\omega_0 kt) \\ \sin(\omega_0 kt) & \cos(\omega_0 kt) \end{pmatrix}, \quad \mathbf{J} = \begin{pmatrix} 0 & -1 \\ 1 & 0 \end{pmatrix}$$

where $V_{s,k}^p, V_{s,k}^n, I_{L,k}^p$ and $I_{L,k}^n$ represent the k -th harmonic coefficient vector for the positive and negative sequence representation of the load current and source voltage, respectively. These coefficient vectors are assumed unknown constants (or slowly varying). $\mathcal{H} = \{1, 3, 5, 7, 11, \dots\}$ is the set of indexes of the harmonic components considered for the compensation, in this case the odd harmonics.

Their time derivative can be explicitly obtained as follows

$$\dot{\mathbf{v}}_{S\alpha\beta} = \mathbf{J}\omega_0 \sum_{k \in \mathcal{H}} (\mathbf{e}^{\mathbf{J}k\omega_0 t} V_{s,k}^p - \mathbf{e}^{-\mathbf{J}k\omega_0 t} V_{s,k}^n) \quad (2.39)$$

$$\frac{d}{dt} \mathbf{i}_{L\alpha\beta} = \mathbf{J}\omega_0 \sum_{k \in \mathcal{H}} (\mathbf{e}^{\mathbf{J}k\omega_0 t} I_{s,k}^p - \mathbf{e}^{-\mathbf{J}k\omega_0 t} I_{s,k}^n) \quad (2.40)$$

- A5. According to the parameters used in practice for the design of these systems, the source current dynamics represent by (2.25) and (2.26) in the system model, respond considerably faster than the dynamics describing the capacitors voltages (2.27) and (2.28). Therefore, the currents dynamics and the voltages dynamics on each subsystem, either A or B, can be treated separately from each other, thus, facilitating the control design even more.

3. CONTROLLER DESIGN

3.1 Introduction

As established in the previous chapter, the overall system can be split in two subsystems that are decoupled from one another. These subsystems are recalled here for easy of reference.

Subsystem A

$$L \frac{d}{dt} \mathbf{i}_{S\alpha\beta} = \mathbf{v}_{S\alpha\beta} - \boldsymbol{\varepsilon}_{\alpha\beta} + L \frac{d}{dt} \mathbf{i}_{L\alpha\beta} \quad (3.1)$$

$$C \frac{d}{dt} z_4 = 2\boldsymbol{\varepsilon}_{\alpha\beta}^T (\mathbf{i}_{S\alpha\beta} - \mathbf{i}_{L\alpha\beta}) - \frac{2z_4}{R} + \underbrace{2\varepsilon_\gamma (i_{S\gamma} - i_{L\gamma})}_{\text{Periodic disturbance}} \quad (3.2)$$

Subsystem B

$$L \frac{d}{dt} i_{S\gamma} = v_{S\gamma} - \frac{\sqrt{3}}{2} (x_5) - \varepsilon_\gamma + L \frac{d}{dt} i_{L\gamma} \quad (3.3)$$

$$C \frac{d}{dt} x_5 = \sqrt{3} (i_{S\gamma} - i_{L\gamma}) - \frac{x_5}{R} \quad (3.4)$$

Remark 3.1.1. *It is important to notice that subsystem A coincides with the description of the well known three-phase three-wire case, except for a periodic disturbance entering in the z_4 dynamics, whose effect is practically negligible, as z_4 dynamics is considered relatively slow. A solution for this problem has been presented in [22], and will be revisited here for the sake of completeness.*

3.2 Subsystem A

Recall that, a first objective of subsystem A consists in the injection of the necessary compensating current $\mathbf{i}_{\alpha\beta}(t)$ to the line to force the current $\mathbf{i}_{S\alpha\beta}(t)$ to be proportional to the line voltage $\mathbf{v}_{S\alpha\beta}(t)$. This is equivalent to seek for a power factor (PF) close to one. The solution presented in [22] consists in the construction of a control signal $\mathbf{u}_{\alpha\beta}$ that cancels $\mathbf{v}_{S\alpha\beta}$, adds a damping term $\mathbf{K}_1(\mathbf{i}_{S\alpha\beta} - \mathbf{i}_{S\alpha\beta}^*)$ to reinforce stability, and introduces a bank of resonant filters to compensate the harmonic disturbance. A second objective of subsystem A consists in the regulation of the sum of both capacitors x_4 towards a voltage level $2V_d$, or equivalently, to force z_4 to reach a constant reference $2V_d^2$, where V_d represents the reference value for each capacitor. The solution in [22] for this regulation objective consists in proposing a proportional plus integral (PI) controller of limited bandwidth to reconstruct the scalar g . Recall that, g is required to construct the reference $\mathbf{i}_{S\alpha\beta}^*$. To limit the bandwidth of such a PI, the proportional term is affected by a low pass filter (LPF) to reduce the effect of the distortion present in z_4 .

According to the decoupling assumption A5, subsystem A can be split, as well, in two parts, which can be treated separately. Hence, the controller for this subsystem is composed of two loops, namely, inner (current) control loop and outer (voltage) control loop, just as in the conventional controller.

3.2.1 Inner control loop

Consider the current dynamics (3.1). In the known parameters case, and according to the *energy shaping plus damping injection* (ESDI) procedure proposed in [23], a copy of subsystem (2.25) is performed. Then, the state $\mathbf{i}_{S\alpha\beta}$ is replaced by its reference $\mathbf{i}_{S\alpha\beta}^*$ and, finally, a damping term is added. This yields the expression

$$L \frac{d}{dt} \mathbf{i}_{S\alpha\beta}^* = L \frac{d}{dt} \mathbf{i}_{L\alpha\beta} - \boldsymbol{\varepsilon}_{\alpha\beta} + \mathbf{v}_{S\alpha\beta} + \mathbf{K}_1 \tilde{\mathbf{i}}_{S\alpha\beta} \quad (3.5)$$

where $\tilde{\mathbf{i}}_{S\alpha\beta} = \mathbf{i}_{S\alpha\beta} - \mathbf{i}_{S\alpha\beta}^*$ is the current tracking error, and \mathbf{K}_1 a positive-definite damping matrix used to introduce the required damping.

Solving (3.5) for $\boldsymbol{\varepsilon}_{\alpha\beta}$, the following controller can be proposed in the case of known parameters

$$\boldsymbol{\varepsilon}_{\alpha\beta} = -L \frac{d}{dt} \mathbf{i}_{S\alpha\beta}^* + L \frac{d}{dt} \mathbf{i}_{L\alpha\beta} + \mathbf{v}_{S\alpha\beta} + \mathbf{K}_1 \tilde{\mathbf{i}}_{S\alpha\beta} \quad (3.6)$$

Notice that, subsystem (3.1) in closed loop with the controller (3.6) yields the following exponentially stable error model

$$L \frac{d}{dt} \tilde{\mathbf{i}}_{S\alpha\beta} = -\mathbf{K}_1 \tilde{\mathbf{i}}_{S\alpha\beta}$$

that is, the controller (3.6) guarantees exponential tracking of $\mathbf{i}_{S\alpha\beta}$ toward the reference $\mathbf{i}_{S\alpha\beta}^*$.

The unknown parameter case

The previous solution is, however, not realizable as inductance L and the time derivatives in (3.6) are unknown. To overcome this issue, it is proposed to lump together all unknown periodic disturbances in a single vector, and to estimate this vector of periodic disturbances by means of adaptation. The reconstruction of such a periodic term can be considerably facilitated if it is assumed that this vector can be represented as a sum of harmonic components, that is, appealing assumption A4.

In what follows, the expressions of the different periodic disturbances are described, and then they are lumped in a single disturbance vector, as proposed above. For this, the time derivative $\frac{d}{dt} \mathbf{i}_{S\alpha\beta}^*$ is computed based on (2.33) and (2.39) as follows

$$\begin{aligned} \frac{d\mathbf{i}_{S\alpha\beta}^*}{dt} &= g \frac{d\mathbf{v}_{S\alpha\beta}}{dt} + \dot{g} \mathbf{v}_{S\alpha\beta} \\ &= \sum_{k \in \mathcal{H}} \left[e^{\mathbf{J}k\omega_0 t} (\dot{g} + g\mathbf{J}k\omega) \mathbf{V}_{S,k}^p + e^{-\mathbf{J}k\omega_0 t} (\dot{g} - g\mathbf{J}k\omega) \mathbf{V}_{S,k}^n \right] \end{aligned} \quad (3.7)$$

Direct substitution of (2.40) and (3.7) in controller (3.6) yields

$$\begin{aligned} \boldsymbol{\varepsilon}_{\alpha\beta} &= - \sum_{k \in \mathcal{H}} e^{\mathbf{J}k\omega_0 t} L (\dot{g} \mathbf{V}_{S,k}^p + g\mathbf{J}k\omega \mathbf{V}_{S,k}^p - \mathbf{J}k\omega \mathbf{I}_{S,k}^p) \\ &\quad - \sum_{k \in \mathcal{H}} e^{-\mathbf{J}k\omega_0 t} (-\dot{g} \mathbf{V}_{S,k}^n + g\mathbf{J}k\omega \mathbf{V}_{S,k}^n + \mathbf{J}k\omega \mathbf{I}_{S,k}^n) \\ &\quad + \mathbf{v}_{S\alpha\beta} + \mathbf{K}_1 \tilde{\mathbf{i}}_{S\alpha\beta} \end{aligned}$$

which can be reduced to

$$\boldsymbol{\varepsilon}_{\alpha\beta} = - \sum_{k \in \mathcal{H}} (\mathbf{e}^{\mathbf{J}k\omega_0 t} \boldsymbol{\Phi}_k^p + \mathbf{e}^{-\mathbf{J}k\omega_0 t} \boldsymbol{\Phi}_k^n) + \mathbf{v}_{S\alpha\beta} + \mathbf{K}_1 \tilde{\mathbf{i}}_{S\alpha\beta} \quad (3.8)$$

where the harmonic coefficients have been lumped according to the following definitions

$$\begin{aligned} \boldsymbol{\Phi}_k^p &\triangleq L(\dot{g}\mathbf{V}_{S,k}^p + g\mathbf{J}k\omega\mathbf{V}_{S,k}^p - \mathbf{J}k\omega\mathbf{I}_{S,k}^p) \\ \boldsymbol{\Phi}_k^n &\triangleq L(-\dot{g}\mathbf{V}_{S,k}^n + g\mathbf{J}k\omega\mathbf{V}_{S,k}^n + \mathbf{J}k\omega\mathbf{I}_{S,k}^n), \quad k \in \mathcal{H} \end{aligned}$$

Consider that g (which is computed later in the voltage loop) is constructed in such a way that, it converges very slowly towards a constant value. Therefore, its time derivative \dot{g} can be practically neglected. As a result, the harmonic coefficients $\boldsymbol{\Phi}_k^p$ and $\boldsymbol{\Phi}_k^n$ ($k \in \mathcal{H}$) can be considered almost constant vectors, or that vary very slowly. Hence, an adaptation scheme can be used to reconstruct such harmonic coefficients, which in their turn can be used to reconstruct the periodic disturbance. This is explained next.

Based on the form of controller (3.8), the following controller that considers estimates for the harmonic coefficients of the periodic disturbance is proposed

$$\boldsymbol{\varepsilon}_{\alpha\beta} = - \sum_{k \in \mathcal{H}} (\mathbf{e}^{\mathbf{J}k\omega_0 t} \hat{\boldsymbol{\Phi}}_k^p + \mathbf{e}^{-\mathbf{J}k\omega_0 t} \hat{\boldsymbol{\Phi}}_k^n) + \mathbf{v}_{S\alpha\beta} + \mathbf{K}_1 \tilde{\mathbf{i}}_{S\alpha\beta} \quad (3.9)$$

where the notation $\widehat{(\cdot)}$ represents the estimate of (\cdot) .

Subsystem (3.1) in closed loop with controller (3.9) yields the following error dynamics

$$L \frac{d}{dt} \tilde{\mathbf{i}}_{S\alpha\beta} = \sum_{k \in \mathcal{H}} (\mathbf{e}^{\mathbf{J}k\omega_0 t} \tilde{\boldsymbol{\Phi}}_k^p + \mathbf{e}^{-\mathbf{J}k\omega_0 t} \tilde{\boldsymbol{\Phi}}_k^n) - \mathbf{K}_1 \tilde{\mathbf{i}}_{S\alpha\beta} \quad (3.10)$$

where $\tilde{\boldsymbol{\Phi}}_k^p \triangleq \hat{\boldsymbol{\Phi}}_k^p - \boldsymbol{\Phi}_k^p = -\boldsymbol{\Phi}_k^p$ and $\tilde{\boldsymbol{\Phi}}_k^n = \hat{\boldsymbol{\Phi}}_k^n - \boldsymbol{\Phi}_k^n = -\boldsymbol{\Phi}_k^n$ represent the parametric errors.

Now, following a Lyapunov approach [24], the adaptive laws to reconstruct the estimates $\hat{\boldsymbol{\Phi}}_k^p$ and $\hat{\boldsymbol{\Phi}}_k^n$ can be proposed. For this purpose, the following simple quadratic function in terms of the square of the tracking and parametric errors is chosen, which is evidently a positive-definite energy storage function.

$$H_1 = \frac{L}{2} \tilde{\mathbf{i}}_{S\alpha\beta}^\top \tilde{\mathbf{i}}_{S\alpha\beta} + \sum_{k \in \mathcal{H}} \frac{1}{2\gamma_k} [(\tilde{\boldsymbol{\Phi}}_k^p)^2 + (\tilde{\boldsymbol{\Phi}}_k^n)^2] \quad (3.11)$$

where $\gamma_k > 0$ ($k \in \mathcal{H}$) are design parameters representing the adaptation gains.

Its time derivative along the trajectories of (3.10) is given by

$$\dot{H}_1 = -\mathbf{K}_1 \tilde{\mathbf{i}}_{S\alpha\beta}^\top \tilde{\mathbf{i}}_{S\alpha\beta} - \tilde{\mathbf{i}}_{S\alpha\beta}^\top \sum_{k \in \mathcal{H}} (e^{\mathbf{J}\omega_0 kt} \tilde{\Phi}_k^p + e^{-\mathbf{J}\omega_0 kt} \tilde{\Phi}_k^n) + \sum_{k \in \mathcal{H}} \frac{1}{\gamma_k} [(\tilde{\Phi}_k^p)^\top \dot{\tilde{\Phi}}_k^p + (\tilde{\Phi}_k^n)^\top \dot{\tilde{\Phi}}_k^n] \quad (3.12)$$

Equation (3.12) is made negative semidefinite, i.e., it is forced to be non increasing by proposing the following adaptive laws

$$\dot{\tilde{\Phi}}_k^p = -\gamma_k e^{-\mathbf{J}\omega_0 kt} \tilde{\mathbf{i}}_{S\alpha\beta} \quad , \quad k \in \mathcal{H} \quad (3.13)$$

$$\dot{\tilde{\Phi}}_k^n = -\gamma_k e^{\mathbf{J}\omega_0 kt} \tilde{\mathbf{i}}_{S\alpha\beta} \quad , \quad k \in \mathcal{H} \quad (3.14)$$

where $\dot{\tilde{\Phi}}_k^p = \dot{\hat{\Phi}}_k^p$ and $\dot{\tilde{\Phi}}_k^n = \dot{\hat{\Phi}}_k^n$ ($k \in \mathcal{H}$), as Φ_k^p and Φ_k^n are considered constants.

The time derivative (3.12) is thus reduced to

$$\dot{H}_1 = -\mathbf{K}_1 \tilde{\mathbf{i}}_{S\alpha\beta}^\top \tilde{\mathbf{i}}_{S\alpha\beta}$$

Since H_1 is radially unbounded, and $\dot{H}_1 \leq 0$ then $\tilde{\mathbf{i}}_{S\alpha\beta} \in \mathcal{L}_2 \cup \mathcal{L}_\infty$, $\tilde{\Phi}_k^p \in \mathcal{L}_\infty$ and $\tilde{\Phi}_k^n \in \mathcal{L}_\infty$ for every $k \in \mathcal{H}$. From (3.10) $\dot{\tilde{\mathbf{i}}}_{S\alpha\beta} \in \mathcal{L}_\infty$. Now, since $\tilde{\mathbf{i}}_{S\alpha\beta} \in \mathcal{L}_\infty$ and $\dot{\tilde{\mathbf{i}}}_{S\alpha\beta} \in \mathcal{L}_\infty$, then $\tilde{\mathbf{i}}_{S\alpha\beta}$ is uniformly continuous, which together with the fact that $\tilde{\mathbf{i}}_{S\alpha\beta} \in \mathcal{L}_2$ imply that $\tilde{\mathbf{i}}_{S\alpha\beta} \rightarrow 0$ asymptotically. Out of this $\tilde{\Phi}_k^p$ and $\tilde{\Phi}_k^n$ equal constant vectors $\forall k \in \mathcal{H}$. However, for $\tilde{\mathbf{i}}_{S\alpha\beta} = 0$ and from (3.10) $\sum_{k \in \mathcal{H}} (e^{\mathbf{J}k\omega_0 t} \tilde{\Phi}_k^p + e^{-\mathbf{J}k\omega_0 t} \tilde{\Phi}_k^n) = 0$, it is clear that the only possible solution is $\tilde{\Phi}_k^p \rightarrow 0$ and $\tilde{\Phi}_k^n \rightarrow 0$.

To avoid the cumbersome rotations of the form $e^{\pm \mathbf{J}\omega kt}$ appearing in the controller above proposed, the following transformations are considered

$$\hat{\phi}_k^p = -\gamma_k e^{-\mathbf{J}\omega_0 kt} \hat{\Phi}_k^p \quad , \quad k \in \mathcal{H}$$

$$\hat{\phi}_k^n = -\gamma_k e^{\mathbf{J}\omega_0 kt} \hat{\Phi}_k^n \quad , \quad k \in \mathcal{H}$$

Out of these transformations, the inner loop controller can be rewritten as

$$\varepsilon_{\alpha\beta} = \sum_{k \in \mathcal{H}} (\hat{\phi}_k^p + \hat{\phi}_k^n) + \mathbf{v}_{S\alpha\beta} + \mathbf{K}_1 \tilde{\mathbf{i}}_{S\alpha\beta} \quad (3.15)$$

with adaptive laws (3.13) and (3.14) now transformed to

$$\dot{\hat{\phi}}_k^p = \gamma_k \tilde{\mathbf{i}}_{S\alpha\beta} - \mathbf{J}k\omega_0 \hat{\phi}_k^p, \quad k \in \mathcal{H} \quad (3.16)$$

$$\dot{\hat{\phi}}_k^n = \gamma_k \tilde{\mathbf{i}}_{S\alpha\beta} - \mathbf{J}k\omega_0 \hat{\phi}_k^n, \quad k \in \mathcal{H} \quad (3.17)$$

Writing the dynamical part of the controller above in its transfer function form, and defining $\hat{\phi}_{\alpha\beta} \triangleq (\hat{\phi}_k^p + \hat{\phi}_k^n)$, $\hat{\phi}_{\alpha\beta} \in \mathbb{R}^2$, the following expressions are obtained

$$\boldsymbol{\varepsilon}_{\alpha\beta} = \sum_{k \in \mathcal{H}} (\hat{\phi}_{k,\alpha\beta}) + \mathbf{v}_{S\alpha\beta} + \mathbf{K}_1 \tilde{\mathbf{i}}_{S\alpha\beta} \quad (3.18)$$

$$\hat{\phi}_{k,\alpha\beta} = \frac{2\gamma_k s}{s^2 + k^2\omega_0^2} \tilde{\mathbf{i}}_{S\alpha\beta}, \quad k \in \mathcal{H} \quad (3.19)$$

where s represents the Laplace complex variable.

Remark 3.2.1. Notice that, the resulting controller includes a bank of resonant filters, each of them tuned at the frequency of the selected harmonic component to be compensated [25].

3.2.2 Outer control loop

For the solution of the voltage regulation loop, the dynamics (3.2) is considered. It is recalled here below for the sake of easy of reference.

$$C\dot{z}_4 = 2\boldsymbol{\varepsilon}_{\alpha\beta}^\top (\mathbf{i}_{s\alpha\beta} - \mathbf{i}_{L\alpha\beta}) - \frac{2z_4}{R} + \underbrace{2\varepsilon_\gamma (i_{s\gamma} - i_{L\gamma})}_{\text{Periodic disturbance}}$$

where, as previously defined $z_4 \triangleq \frac{x_4^2}{2}$, and $x_4 \triangleq v_{C1} + v_{C2}$.

The main objective of this outer control loop consists in regulating the dc component of x_4 towards a predefined constant reference $2V_d$ (V_d is taken as a reference for each capacitor). Notice, however, that due to the transformation, this control objective has been translated to force the dc component of z_4 to reach a constant value $2V_d^2$.

According to the decoupling assumption **A5**, it is assumed that the current dynamics are much faster than the voltage dynamics. Hence, it can be assumed that,

after a relatively short time, the source current is practically tracking its reference, that is, $\mathbf{i}_{S\alpha\beta} \cong \mathbf{i}_{S\alpha\beta}^* = g\mathbf{v}_{S\alpha\beta}$ and $\hat{\phi}_{k,\alpha\beta} \cong \phi_{k,\alpha\beta}$.

Under these assumptions, making a direct substitution of control (3.18) in the dynamics (3.2), and after some simple manipulations the following expressions are obtained

$$\begin{aligned}
C \frac{d}{dt} z_4 &= 2 \underbrace{\left[\sum_{k \in \mathcal{H}} (\hat{\phi}_{k,\alpha\beta}) + \mathbf{v}_{S\alpha\beta} + \mathbf{K}_1 \tilde{\mathbf{i}}_{S\alpha\beta} \right]}_{\varepsilon_{\alpha\beta}} (\mathbf{i}_{S\alpha\beta} - \mathbf{i}_{L\alpha\beta}) - \frac{2z_4}{R} + 2\varepsilon_\gamma (i_{S\gamma} - i_{L\gamma}) \\
&= 2 \left[\sum_{k \in \mathcal{H}} (\phi_{k,\alpha\beta}) + \mathbf{v}_{S\alpha\beta} \right] (g\mathbf{v}_{S\alpha\beta} - \mathbf{i}_{L\alpha\beta}) - \frac{2z_4}{R} + 2\varepsilon_\gamma (i_{S\gamma} - i_{L\gamma}) \\
&= g(2\mathbf{v}_{S\alpha\beta}^\top \sum_{k \in \mathcal{H}} (\phi_{k,\alpha\beta}) + 2\mathbf{v}_{S\alpha\beta}^\top \mathbf{v}_{S\alpha\beta}) - 2\mathbf{i}_{L\alpha\beta}^\top \sum_{k \in \mathcal{H}} (\phi_{k,\alpha\beta}) - 2\mathbf{i}_{L\alpha\beta}^\top \mathbf{v}_{S\alpha\beta} \\
&\quad - \frac{2z_4}{R} + 2\varepsilon_\gamma (i_{S\gamma} - i_{L\gamma})
\end{aligned}$$

Remark 3.2.2. *It is clear that, as a result of the harmonic distortion compensation, and due to the charging mechanism for the capacitors, the resulting capacitor voltage will be naturally and unavoidable polluted by high order harmonics in the form of a relatively small ripple. The compensation of this ripple is out of the scope of the present work. The regulation objective is thus limited to regulate the mean value of the capacitor voltage towards a constant reference, while maintaining the ripple bounded and as small as possible.*

As this control loop is focused on the regulation of the dc component of z_4 , it is proposed to extract such a dc component applying the following average function, which filters out the high order harmonic component from the system variables.

$$\langle x \rangle_0 = \frac{1}{T} \int_{t-T}^t x(\tau) d\tau$$

The following expression is obtained after application of the averaging operation

$$C \dot{\tilde{z}}_4 = gc_1 - \frac{2\tilde{z}_4}{R} + c_2 \quad (3.20)$$

where $\tilde{z}_4 = z_4 - z_4^*$, $z_4^* = V_d^2/2$ and $\dot{\tilde{z}}_4 = \dot{z}_4$ and the constants c_1 and c_2 are given by

$$\begin{aligned} c_1 &= \langle 2\mathbf{v}_{S\alpha\beta}^\top \sum_{k \in \mathcal{H}} (\boldsymbol{\phi}_{k,\alpha\beta}) + 2\mathbf{v}_{S\alpha\beta}^\top \mathbf{v}_{S\alpha\beta} \rangle_0 \\ c_2 &= \langle 2\mathbf{i}_{L\alpha\beta}^\top \sum_{k \in \mathcal{H}} (\boldsymbol{\phi}_{k,\alpha\beta}) + 2\mathbf{i}_{L\alpha\beta}^\top \mathbf{v}_{S\alpha\beta} - 2\varepsilon_\gamma (i_{S\gamma} - i_{L\gamma}) \rangle_0 - \frac{V_d^2}{2} \end{aligned}$$

which are assumed to be unknown.

Remark 3.2.3. Notice that, in normal operation $|\mathbf{v}_{S\alpha\beta}^\top \sum_{k \in \mathcal{H}} (\boldsymbol{\phi}_{k,\alpha\beta})| \ll |\mathbf{v}_{S\alpha\beta}^\top \mathbf{v}_{S\alpha\beta}|$ therefore $c_1 > 0$. Indeed $c_1 \cong \langle \mathbf{v}_{S\alpha\beta}^\top \mathbf{v}_{S\alpha\beta} \rangle_0 = v_{S,RMS}^2$

The system (3.20) is a first-order linear time invariant (LTI) system, with output \tilde{z}_4 , the signal g is the control input affected by the positive constant c_1 , and the unknown constant signal c_2 as a constant perturbation. The control design of this “outer loop” should include a damping term to reinforce the asymptotic stability for the closed loop system, and should incorporate robustness to reject parametric uncertainties. In this case, a simple proportional plus integral (PI) controller can solve the problem since the perturbation is simply an unknown constant.

Remark 3.2.4. It is proposed to substitute the proportional of PI controller by a low-pass filter since the direct use of \tilde{z}_4 could introduce more harmonics distortion in the computation of g which would be reinjected to the system by means of $\mathbf{i}_{S\alpha\beta}^*$.

The proposed controller is given by

$$v_{S,RMS}^2 g = -\frac{k'_{i1}}{s} \tilde{z}_4 - \frac{k'_{p1}}{\tau_1 s + 1} \tilde{z}_4 \quad (3.21)$$

where k'_{p1} , k'_{i1} and τ_1 are positive design parameters. Notice that, this error of the squares can be expressed as $\tilde{z}_4 = \frac{1}{2}(x_4 + 2V_d)(x_4 - 2V_d)$. Assuming that x_4 is bounded away from zero and close to $2V_d$, then the error can be approximated with $\tilde{z}_4 \cong 2V_d(x_4 - 2V_d)$, and thus, a simpler form of the voltage regulation loop can be obtained as follows

$$v_{S,RMS}^2 g = -\frac{k_{i1}}{s} \tilde{x}_4 - \frac{k_{p1}}{\tau_1 s + 1} \tilde{x}_4 \quad (3.22)$$

where $\tilde{x}_4 = (x_4 - 2V_d)$, and the design parameters are related according to $k_{i1} = 2V_d k'_{i1}$ and $k_{p1} = 2V_d k'_{p1}$.

The block diagram of the controller for subsystem A is shown in Fig. 3.1.

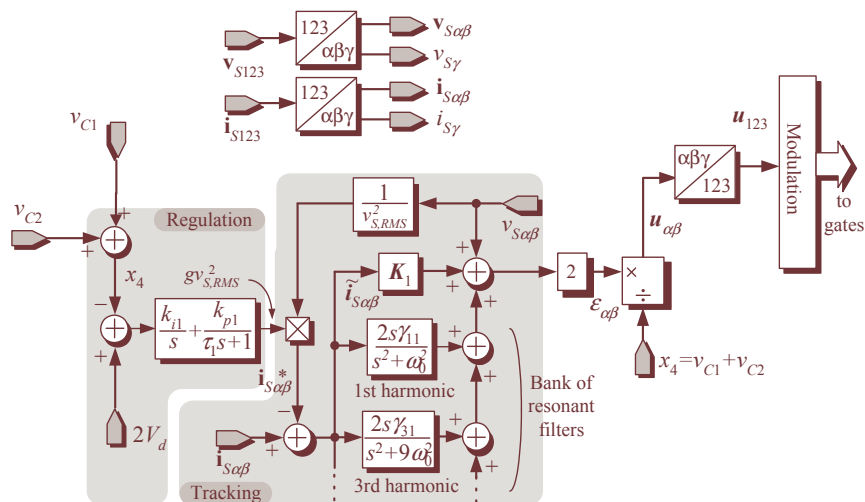


Figure 3.1 Block Diagram of the control (Subsystem A).

3.3 Subsystem B

Subsystem B describes the dynamics of the homopolar component of the source current and the dynamic of the capacitor voltages difference. These equations are recalled here below for easy of reference.

$$L \frac{d}{dt} i_{S\gamma} = v_{S\gamma} - \frac{\sqrt{3}}{2} (x_5) - \varepsilon_\gamma + \underbrace{L \frac{d}{dt} i_{L\gamma}}_{\text{harmonic distortion}} \quad (3.23)$$

$$C \frac{d}{dt} x_5 = \sqrt{3} i_{S\gamma} - \frac{x_5}{R} - \underbrace{\sqrt{3} i_{L\gamma}}_{\text{harmonic distortion}} \quad (3.24)$$

Notice that, this is a controllable second order system perturbed by a certain offset (perhaps due to measurements errors) plus harmonic distortion appearing in both rows of the subsystem B.

The following controller that cancels $v_{S\gamma}$, adds a damping term of the form $k_2 i_{S\gamma}$ and includes a term \hat{v} related with the rejection of the harmonic distortion is proposed. Notice, also it is included a proportional term in x_5 of limited bandwidth to reduce

the reinjection of more distortion appearing in x_5

$$\varepsilon_\gamma = v_{S\gamma} + k_{p2}\chi_5 + k_2 i_{S\gamma} + \hat{\vartheta} \quad (3.25)$$

$$\tau_2 \dot{\chi}_5 = x_5 - \chi_5 \quad (3.26)$$

where k_2 and k_{p2} are the proportional gains and τ_2 is the time constant of the LPF.

Remark 3.3.1. *As before, appealing assumption A4, it is considered that the γ coordinate of load current $i_{L\gamma}$ is a periodic signal containing higher harmonics of the fundamental frequency ω_0 , and thus it can be represented as the following sum*

$$i_{L\gamma} = \sum_{m \in \mathcal{H}_2} \boldsymbol{\rho}_m^\top \mathbf{I}_m$$

where $\boldsymbol{\rho}_m$ is a rotation vector of the form

$$\boldsymbol{\rho}_m = \begin{pmatrix} \cos(m\omega_0 t) \\ \sin(m\omega_0 t) \end{pmatrix} \quad (3.27)$$

$$\boldsymbol{\rho}_m^{-1} = (\boldsymbol{\rho}_m)^\top$$

$\mathbf{I}_m \in \mathbb{R}^2$ represents a vector of the m -th harmonic coefficients, all load current harmonic coefficients vectors \mathbf{I}_m are assumed to be unknown constants, and \mathcal{H}_2 is the set of the selected harmonics indices, i.e., $m \in \mathcal{H}_2 = \{1, 3, 5, 7, 9, \dots\}$. Based on this assumption, the time derivative of $i_{L\gamma}$ can be explicitly represented as follows

$$\frac{d}{dt} i_{L\gamma} = -\omega_0 \sum_{m \in \mathcal{H}_2} m \boldsymbol{\rho}_m^\top \mathbf{J} \mathbf{I}_m \quad , \quad \mathbf{J} = \begin{pmatrix} 0 & -1 \\ 1 & 0 \end{pmatrix}$$

The state-space representation of controller (3.25) and (3.26) in closed loop with the subsystems (3.3) and (3.4) gives the following dynamics

$$\begin{pmatrix} \frac{d}{dt} i_{S\gamma} \\ \dot{x}_5 \\ \dot{\chi}_5 \end{pmatrix} = \begin{pmatrix} -\frac{k_2}{L} & -\frac{\sqrt{3}}{2L} & -\frac{k_{p2}}{L} \\ \frac{\sqrt{3}}{C} & -\frac{1}{RC} & 0 \\ 0 & \frac{1}{\tau_2} & -\frac{1}{\tau_2} \end{pmatrix} \begin{pmatrix} i_{S\gamma} \\ x_5 \\ \chi_5 \end{pmatrix} + \begin{pmatrix} 1 \\ 0 \\ 0 \end{pmatrix} \hat{\vartheta} + \begin{pmatrix} -1 & 0 \\ 0 & -\frac{\sqrt{3}}{C} \\ 0 & 0 \end{pmatrix} \begin{pmatrix} \psi \\ i_{L\gamma} \end{pmatrix} \quad (3.28)$$

where, according to remark 3.3.1,

$$\psi = L \frac{d}{dt} i_{L\gamma} = -\omega_0 \sum_{m \in \mathcal{H}_2} m \boldsymbol{\rho}_m^\top \mathbf{J} \mathbf{I}_m \quad , \quad i_{L\gamma} = \sum_{m \in \mathcal{H}_2} \boldsymbol{\rho}_m^\top \mathbf{I}_m$$

are considered two periodic disturbances.

3.3.1 Unperturbed System

Following a classical tools such as the Routh-Hurwitz criterion [26], it is easy to see that the equilibrium point of the unperturbed system given by $[\bar{i}_{S\gamma}, \bar{x}_5, \bar{\chi}_5]^\top = [0, 0, 0]^\top$ is stable provided if the following inequality is fulfilled

$$k_2 \left(\frac{C}{\tau_2} + \frac{3\tau_2}{2L} \right) + \frac{k_2^2 C}{L} > \sqrt{3} k_{p2} \quad (3.29)$$

where k_2 and k_{p2} are chosen positive.

3.3.2 Disturbance Rejection

As previously mentioned, the space-state representation given by (3.28) collects the dynamics (3.3) and (3.4) in closed loop with the proposed controller (3.25), where ϑ appears as the new control input, and ψ and $i_{L\gamma}$ represent two disturbances. This problem can be formulated as a disturbance rejection problem, where unfortunately, the system does not fulfills the matching condition [27], and thus, it is not possible to reject the disturbances effect on the full state. Notice that, the dynamical system (3.28) has harmonic disturbance in both rows, while the control input appears only in the first row. Therefore, the controller proposed here gives priority to the disturbance rejection in $i_{S\gamma}$, that is, the controller (3.37) must be able to drive $i_{S\gamma}$ towards zero, while maintaining the state x_5 as close as possible to zero and only in average, the last means that, a certain amount of ripple and perhaps an imperceptible offset in x_5 are allowed.

The problem is now reduced to compute ϑ to reject the disturbances affecting this system. To facilitate the design of the control signal $\hat{\phi}$, it is convenient to define the following transformations

$$\begin{aligned} \tilde{x}_5 &= x_5 + \varphi_1 \\ \tilde{\chi}_5 &= \chi_5 + \varphi_2 \end{aligned}$$

where φ_1 and φ_2 are two periodic bounded signals constructed according to the following stable filter

$$\begin{aligned} C\dot{\varphi}_1 &= \sqrt{3}i_{L\gamma} - \frac{\varphi_1}{R} \\ \tau_2\dot{\varphi}_2 &= \varphi_1 - \varphi_2 \end{aligned}$$

Direct substitution of above expression in 3.28 yields the following system

$$L \frac{di_{S\gamma}}{dt} = -\frac{\sqrt{3}\tilde{x}_5}{2} - k_2 i_{S\gamma} - k_{p2}\tilde{\chi}_5 + \vartheta - \hat{\vartheta} \quad (3.30)$$

$$C\dot{\tilde{x}}_5 = \sqrt{3}i_{S\gamma} - \frac{\tilde{x}_5}{R} \quad (3.31)$$

$$\tau_2\dot{\tilde{\chi}}_5 = x_5 - \tilde{\chi}_5 \quad (3.32)$$

where $\vartheta = (\psi + \frac{\sqrt{3}}{2}\varphi_1 + k_{p2}\varphi_2)$ is a term that concentrates all periodic disturbances. This disturbance term appears only in the first row, and has the same harmonic contents as $i_{L\gamma}$. The transfer function from $(\phi - \hat{\phi})$ to $i_{S\gamma}$ is given by

$$i_{S\gamma} = G(s)(\vartheta - \hat{\vartheta}) \quad (3.33)$$

$$G(s) = \frac{(s + \frac{1}{RC})(s + \frac{1}{\tau_2})}{(s + \frac{k_2}{L})(s + \frac{1}{RC})(s + \frac{1}{\tau_2}) + \frac{3}{2LC}(s + \frac{1}{\tau_2}) + \frac{\sqrt{3}k_{p2}}{\tau_2 LC}}$$

where s represents the Laplace complex variable. Notice that, the transfer function $G(s)$ is stable provided condition (3.29) is fulfilled. It is proposed to build the control input $\hat{\vartheta}$ as follows

$$\hat{\vartheta} = C(s)i_{S\gamma} \quad (3.34)$$

where $C(s)$ is a transfer function representation of the controller. The design of $C(s)$ is based on the Internal Model Principle [28], which states that the controlled output can reject (track) a class of disturbance (reference commands) without a steady error if the generator (or the model) of the disturbance (reference) is included in the stable closed-loop system. It is well known that the generator of a sinusoidal signal is a harmonic oscillator (resonant filter). Hence, if a periodic reference has an infinite Fourier series (of harmonic components), then an infinite number of resonant filters are required to reject (track) such disturbance (reference), that is, $i_{S\gamma}$ goes to zero if $C(s)$ include the same harmonic content of the disturbances. This motivates the form of the controller presented below

$$C(s) = \sum_{m \in \mathcal{H}_2} \frac{\lambda_m s}{s^2 + m^2 \omega_0^2} \quad (3.35)$$

where λ_m is a positive design parameter. In effect, direct substitution of (3.34) in the expression (3.33), and solving for $i_{S\gamma}$ yields

$$i_{S\gamma} = \frac{G(s)}{1 + G(s)C(s)}\vartheta \quad (3.36)$$

where it is clear that, the poles of the m -th resonant filter in (3.35) become imaginary conjugate zeros in the transfer function (3.36), thus cancelling the corresponding m -th harmonic component of the disturbance ϑ .

Remark 3.3.2. *It is also important to remark that, although it has been somehow assumed that both disturbances $i_{L\gamma}$ and ψ have the same harmonic contents, this is not strictly necessary, in fact, to fulfill the disturbance rejection objective it is necessary to have a resonant filter for all the harmonic components under consideration coming from either disturbance.*

To have an insight of the structure selected for the harmonic compensation scheme (3.35), it is assumed that the current dynamics is faster than the capacitor voltage dynamics, which follows from the decoupling assumption. Therefore, it is proposed to compute $\hat{\vartheta}$ taking into account the dynamics of $i_{S\gamma}$ only, and considering both x_5 and χ_5 as composed of a vanishing perturbation term plus a negligible harmonic disturbance term. Moreover, consider that, the periodic disturbance and the control signal can be rewritten as $\vartheta = \sum_{m \in \mathcal{H}_2} \rho_m^\top \Psi_m$, and $\hat{\vartheta} = \sum_{m \in \mathcal{H}_2} \rho_m^\top \hat{\Psi}_m$, respectively, with ρ_m as defined in (3.27), Ψ_m unknown constant vectors, and $\hat{\Psi}_m$ representing their corresponding estimates to be constructed later. Consider that, controller (3.25) has the following form

$$\varepsilon_\gamma = v_{S\gamma} + k_{p2}\chi_5 + k_2 i_{S\gamma} + \sum_{m \in \mathcal{H}_2} \rho_m^\top \hat{\Psi}_m \quad (3.37)$$

where the control signal has been rewritten as $\hat{\psi} = \sum_{m \in \mathcal{H}_2} \rho_m^\top \hat{\Psi}_m$ with $\hat{\Psi}_m$ representing a control vector, yet to be defined. Subsystem (3.23) in closed loop with controller (3.37) yields the following error dynamics

$$L \frac{d}{dt} i_{S\gamma} = -k_2 i_{S\gamma} - \sum_{m \in \mathcal{H}_2} \rho_m^\top \tilde{\Psi}_m + \epsilon_t \quad (3.38)$$

where it was defined $\tilde{\Psi}_m \triangleq (\hat{\Psi}_m - \Psi_m)$, $m \in \mathcal{H}_2$, and $\epsilon_t = (-\frac{\sqrt{3}}{2}x_5 - k_{p2}\chi_5)$ is a vanishing perturbation.

Next, following the Lyapunov approach [24], the adaptive laws are derived to reconstruct the vector parameter Ψ_m , and thus, to force $\tilde{\Psi}_m \rightarrow 0$ ($m \in \mathcal{H}_2$). For this

reason, the following positive-definite storage function is proposed

$$V_1 = \frac{L}{2} i_{S\gamma}^2 + \sum_{m \in \mathcal{H}_2} \frac{1}{\lambda_m} \tilde{\Psi}_m^\top \tilde{\Psi}_m$$

where λ_m ($m \in \mathcal{H}_2$) are positive design constants which represent the adaptation gains. Its time derivative along the trajectories of (3.38) is given by

$$\dot{V}_1 = -k_2 i_{S\gamma}^2 - i_{S\gamma} \sum_{m \in \mathcal{H}_2} \rho_m^\top \tilde{\Psi}_m + \sum_{m \in \mathcal{H}_2} \frac{1}{\lambda_m} \dot{\tilde{\Psi}}_m^\top \tilde{\Psi}_m + i_{S\gamma} \epsilon_t \quad (3.39)$$

the following adaptive laws can be proposed

$$\dot{\tilde{\Psi}}_m = \lambda_m i_{S\gamma} \rho_m \quad , \quad m \in \mathcal{H}_2 \quad (3.40)$$

where $\dot{\hat{\Psi}}_m = \dot{\tilde{\Psi}}_m$ since Ψ_m is assumed constant. To avoid the cumbersome rotations, the following transformations (rotations) are proposed

$$\hat{\psi}_m = \rho_m^\top \hat{\Psi}_k \quad (3.41)$$

$$\hat{\xi}_m = \rho_m^\top \mathbf{J} \hat{\Psi}_k \quad , \quad m \in \mathcal{H}_2 \quad (3.42)$$

Out of which, the adaptation laws can be rewritten as

$$\dot{\hat{\psi}}_m = \lambda_m i_{S\gamma} - m\omega_0 \hat{\xi}_m \quad (3.43)$$

$$\dot{\hat{\xi}}_m = m\omega_0 \hat{\psi}_m \quad , \quad m \in \mathcal{H}_2 \quad (3.44)$$

which can be written in the form of transfer function as

$$\hat{\psi}_m = \frac{\lambda_m s}{s^2 + m^2 \omega_0^2} i_{S\gamma} \quad , \quad m \in \mathcal{H}_2 \quad (3.45)$$

and thus,

$$\hat{\vartheta} = \sum_{m \in \mathcal{H}_2} \frac{\lambda_m s}{s^2 + m^2 \omega_0^2} i_{S\gamma} \quad (3.46)$$

Finally, direct substitution of (3.46) in control (3.25) yields

$$\varepsilon_\gamma = v_{S\gamma} + k_{p2} \chi_5 + k_2 i_{S\gamma} + \sum_{m \in \mathcal{H}_2} \frac{\lambda_m s}{s^2 + m^2 \omega_0^2} i_{S\gamma} \quad (3.47)$$

$$\tau_2 \dot{\chi}_5 = x_5 - \chi_5 \quad (3.48)$$

Summarizing, the final expressions for the overall controller, including the current tracking loop, the homopolar current compensation, and voltage regulation and balance loops are given by

$$\begin{aligned}
\mathbf{u}_{\alpha\beta} &= \frac{2\varepsilon_{\alpha\beta}}{x_4} & u_\gamma &= \frac{2\varepsilon_\gamma}{x_4} \\
\varepsilon_{\alpha\beta} &= \sum_{k \in \mathcal{H}} \frac{2\gamma_k s}{s^2 + k^2\omega^2} \tilde{\mathbf{i}}_{S\alpha\beta} + \mathbf{v}_{S\alpha\beta} + \mathbf{K}_1 \tilde{\mathbf{i}}_{S\alpha\beta} \\
\tilde{\mathbf{i}}_{S\alpha\beta} &= \mathbf{i}_{S\alpha\beta} - \mathbf{i}_{S\alpha\beta}^* \\
\varepsilon_\gamma &= v_{S\gamma} + k_{p2}\chi_5 + k_2 i_{S\gamma} + \sum_{m \in \mathcal{H}_2} \frac{\lambda_m s}{s^2 + m^2\omega_0^2} i_{S\gamma} \\
\tau_2 \dot{\chi}_5 &= x_5 - \chi_5 \\
g &= -\frac{k_i}{s} \tilde{z}_4 - \frac{k_p a}{s+b} \tilde{z}_4 \\
\tilde{z}_4 &= 2V_d - z_4 \\
z_4 &\triangleq \frac{x_4^2}{2}
\end{aligned}$$

and were presented on [6]. The block diagram of the overall controller is shown in Fig. 3.2.

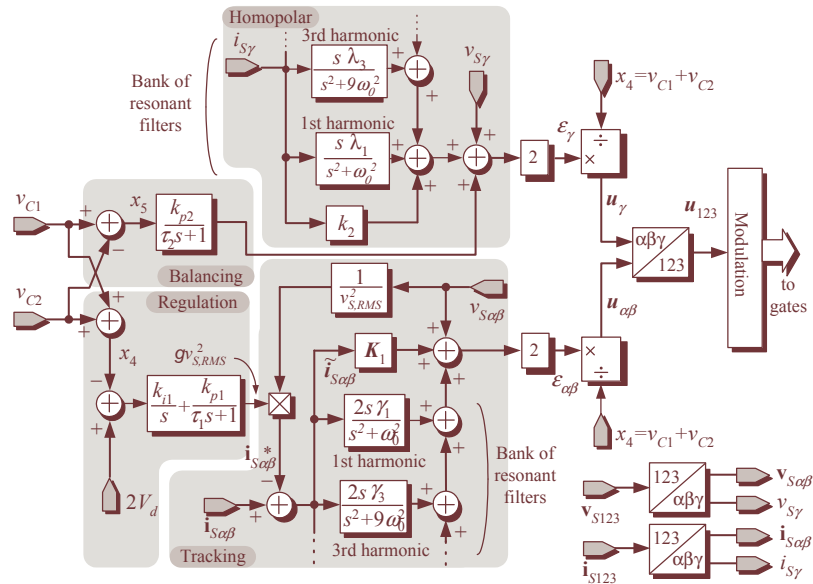


Figure 3.2 Block Diagram of the proposed controller.

4. PHYSICAL IMPLEMENTATION

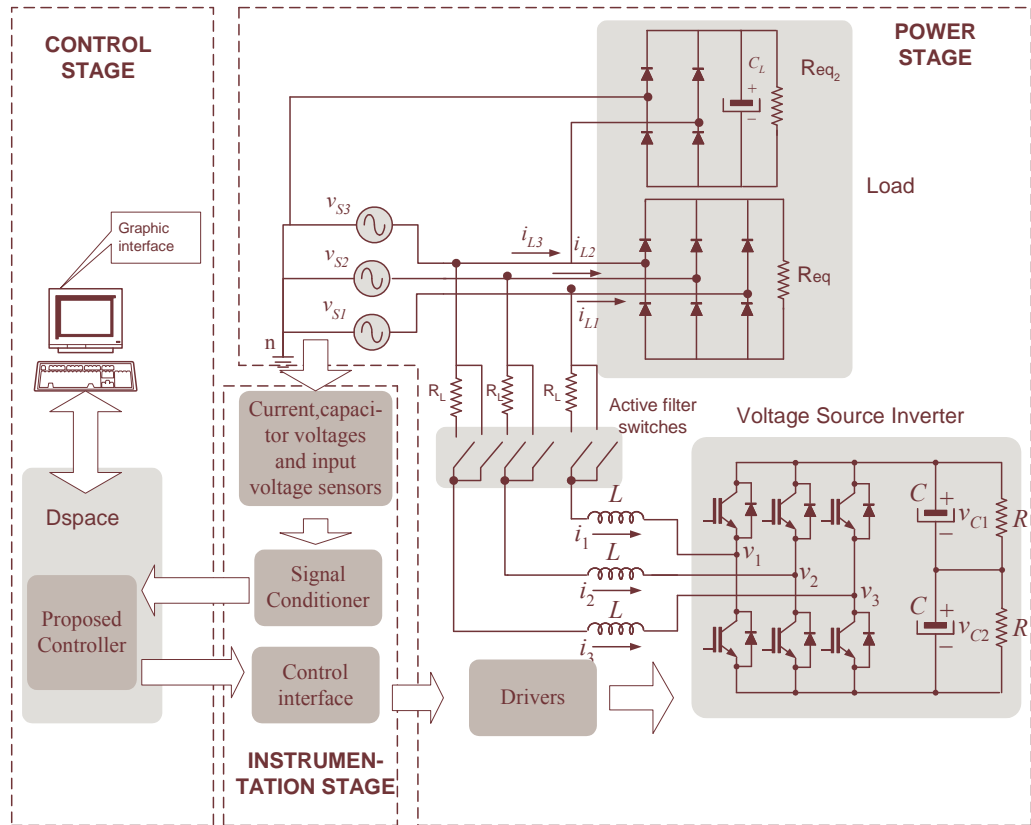


Figure 4.1 Overall scheme of the three-phase four-wire shunt active filter showing the main stages

This chapter describes the implementation of the prototype of a three-phase four-wire shunt active filter studied in this thesis work. The main components of the prototype can be grouped in the following three stages.

1. Power stage - includes the source, the nonlinear load and the active filter.
2. Control stage - composed of the control card on a PC, a control interface, and manoeuvres circuits.
3. Instrumentation stage - includes signal conditioning circuits for current and voltage sensors, as well as voltage limiters.

Figure 4.1 shows the schematic of these stages which are described next. A picture of the final prototype is presented in Fig. 4.2.

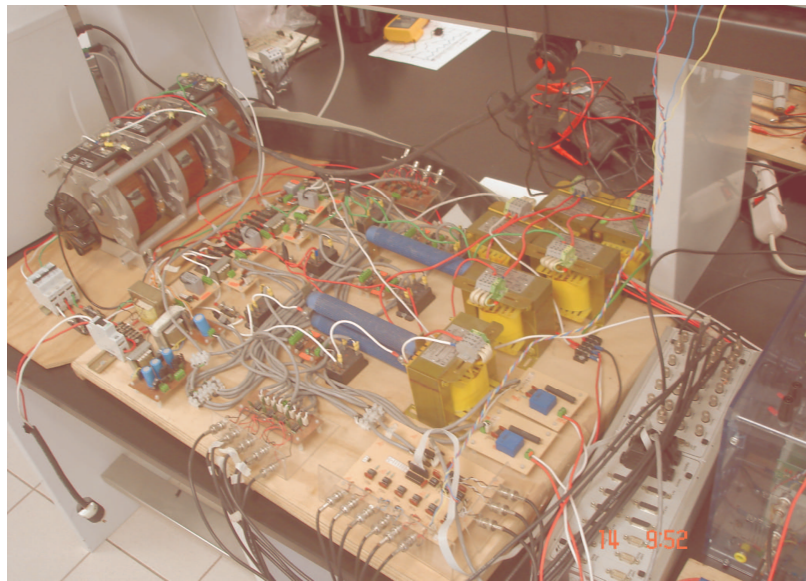


Figure 4.2 Picture of the prototype.

4.1 Power stage

The *power stage* is based on a “Power Electronics Teaching System” produced by SemikronTM which is shown in Fig. 4.3. It includes a VSI composed of three legs of half-bridge modules SKM50-GB123D of insulated gate bipolar transistors (IGBTs) mounted on a heat sink, three drivers SKHI-22A to easily switch on and off the IGBTs, and two capacitors of 2200 μF connected in series on the dc side of the VSI.

All these components are enclosed in an acrylic cabinet, where several connectors have been placed to easily access some interesting connection points of the VSI. Table 4.1 shows the main specifications of this module. To complete the power stage, the VSI is connected to the voltage source by means of three inductances of $L = 5$ mH at 25 A. The power stage is fed by a three-phase variable transformer (variac) in wye with neutral connection. The variac is a 2510-3 type produced by Statco Energy ProductsTM, whose main characteristics are shown in Table 4.2.

VSI	
No over load output current	▶ 30 A
Power Supply (SKHI-22A)	▶ 0-15 V
Capacitors	▶ 2200 μ F (two)
Maximum DC Voltages applied to capacitors	▶ 750 V
Current Consumption (SKHI-22A)	▶ 16 mA
Switching frequency	▶ 20 kHz

Table 4.1 Technical details of the “Power Electronics Teaching System”.

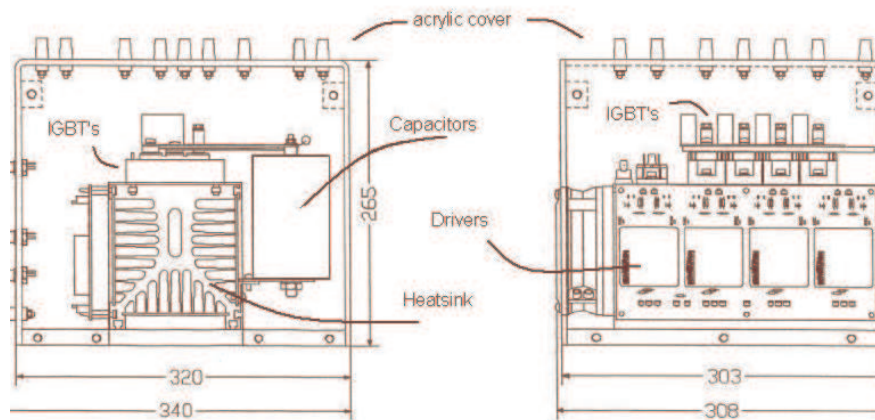


Figure 4.3 “Power Electronics Teaching System”.

The *nonlinear load* is composed of a three phase diode bridge (non-controlled) rectifier model PSD 31/12 made by Power-SemTM, feeding a resistor R_{eq} to produce a non linear load. The resistor can be changed from 145 Ω to 74 Ω to observe

Variac	
Input Voltage	▶ 240 V (line to line voltage)
Input frequency	▶ 50/60 Hz
Output Voltage	▶ 0-280 V (line to line voltage)

Table 4.2 Technical details of the variac 2510-3 type produced by Statco Energy ProductsTM.

the transient responses during load changes. Moreover, a single phase diode bridge rectifier is connected between one phase and the neutral line to produce the homopolar component of the source current, that is, to have a current flowing in the fourth wire, as well as additional unbalance. This single phase rectifier feeds a resistor Req_2 to 300 W and a capacitor of $C_L = 470 \mu\text{F}, 250 \text{ V}$. Resistance Req_2 can be changed from 350Ω to 175Ω 300 W. The overall load is connected and disconnected from the source by means of an array of relays. These relays are controlled by a dSPACETMDS1103 card which is described in the next section. The schematic of the nonlinear load is shown in Fig. 4.4.

The time response of the distorted load current is shown in Fig. 4.5. Its corresponding frequency spectrum is shown in Fig. 4.6. The time response and corresponding frequency spectrum of the homopolar component of the load current is shown in Fig. 4.7.

Remark 4.1.1. *Notice that the load current is composed mainly by odd harmonics of the fundamental frequency f_0 , while the homopolar current is mainly composed by harmonics multiples of three, that is, 3rd, 9th, etc.*

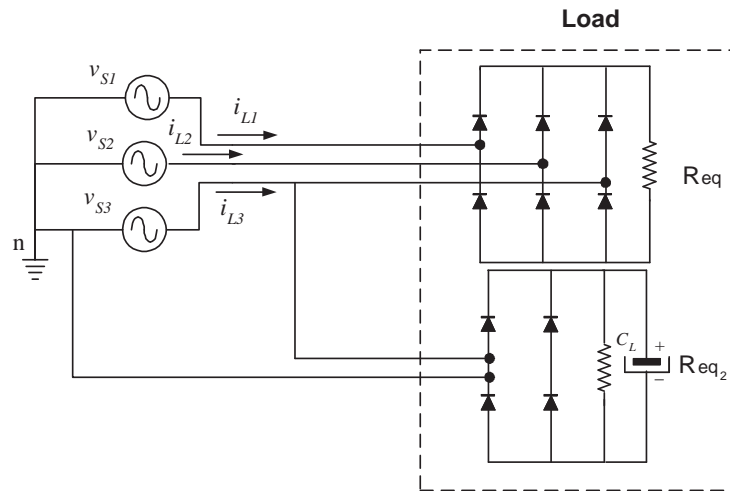


Figure 4.4 Schematic of the distorted unbalanced load.

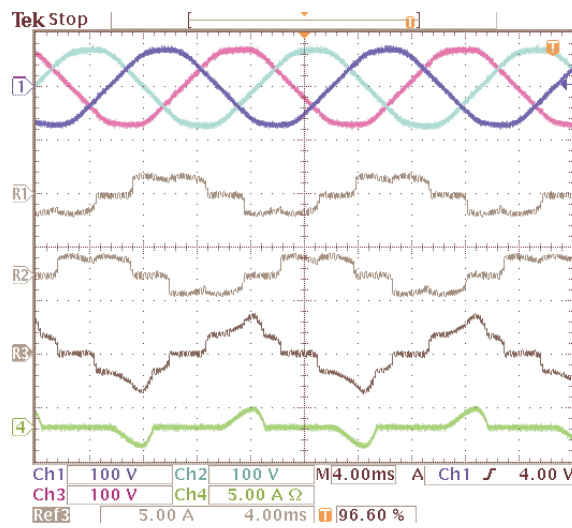


Figure 4.5 (Top plot) Three phase input voltages (x-axis 4 ms/div and y-axis 100 V/div), (four next plots, from top to bottom) the three load currents and the homopolar current (x-axis 4 ms/div and y-axis 5 A/div).

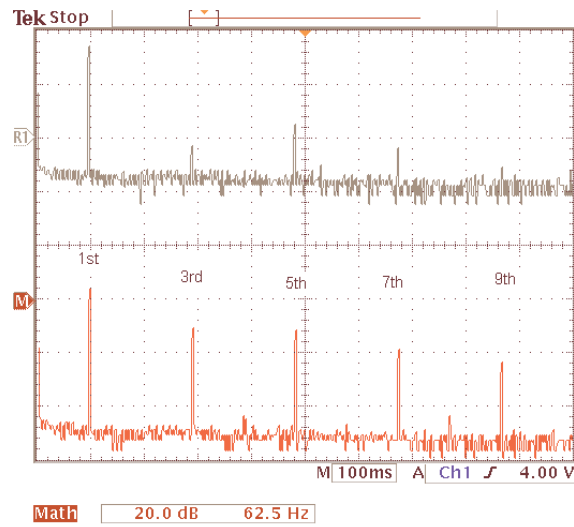


Figure 4.6 Frequency spectrum of (only one phase) (**top**) the source voltage and (**bottom**) the corresponding load current (x-axis 62.5 Hz/div and y-axis 10 dB/div).

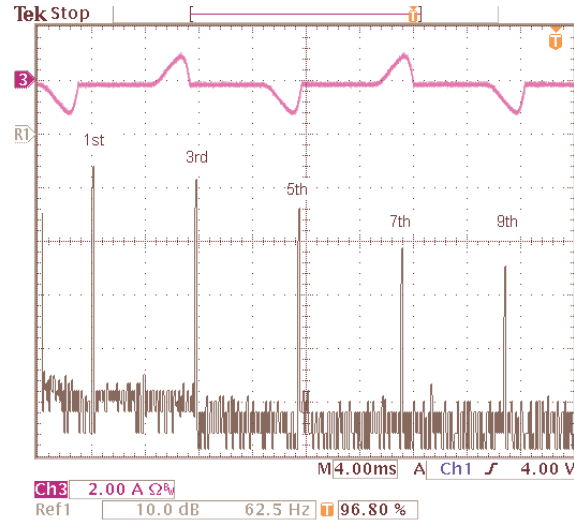


Figure 4.7 (**Top**) Steady state time response of the load current homopolar component (x-axis 4 ms/div and y-axis 2 A/div), and (**bottom**) its frequency spectrum (x-axis 62.5 Hz/div and y-axis 10 dB/div).

4.2 Control stage

The *control stage* is based on a dSPACETM DS1103 card. The DS1103 is a digital signal processor (DSP) over a PC platform where the controller can be easily programmed. The control law is introduced in a Simulink/MATLABTM environment, then compiled and downloaded to the DS1103 card using the Realtime-workshop tools included in the SimulinkTM package. The DS1103 is equipped with a PowerPC processor for fast floating-point calculation at 400 MHz. For special input/output (I/O) tasks, a fixed point DSP TMS320F240 is integrated as a slave subsystem. The main characteristics of the DS1103 are shown in Table 4.3. Figure 4.8 shows the schematic diagram showing the main functions of the DS1103 card.

Technical Details	
Processor	▶ PowerPC 604e / 400 MHz
Timers	▶ 2 general purpose timers
Memory	▶ 2 MByte local SRAM as program memory ▶ 128 MByte global DRAM for data storage and data exchange with host
Interrupt Control Unit	▶ Interrupts by host PC, CAN, slave DSP, serial interface and 4 external inputs (user interrupts)
Analog Input	▶ 4 ADC units 16-bit, multiplexed (4 channels each), sample and hold, 4 μ s sampling time (for 1 channel) ▶ 4 channels 12-bit, sample and hold, 800 ns sampling time ▶ ± 10 V input voltage range
Analog Output	▶ 8 channels 14-bit ▶ ± 10 V input voltage range
Digital I/O	▶ 4 channels 8-bit digital I/O port
Slave DSP Subsystem	▶ Texas Instruments TM DSP TMS320F240, 20 MHz ▶ Three-phase PWM outputs plus 4 single PWM outputs

Table 4.3 Technical details of the DS1103.

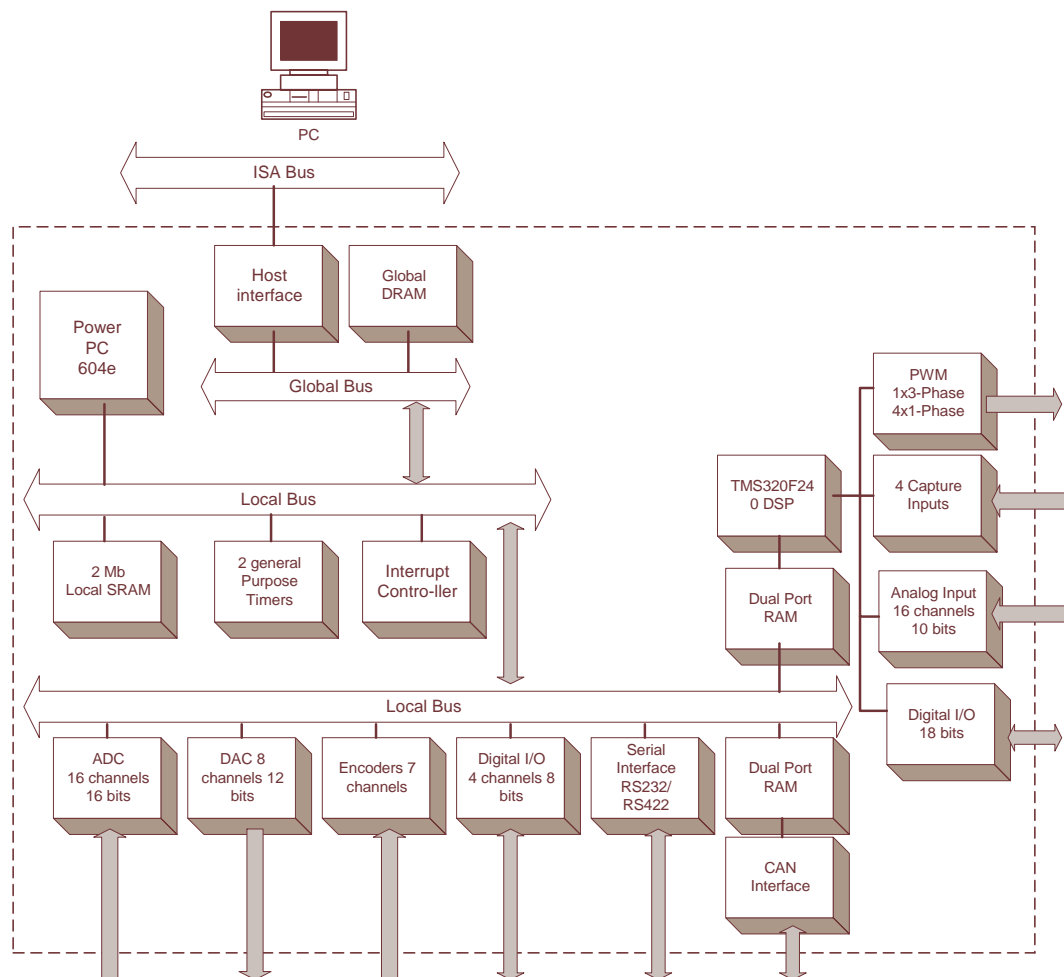


Figure 4.8 Schematic of the different components of the dSPACE™ DS1103 card.

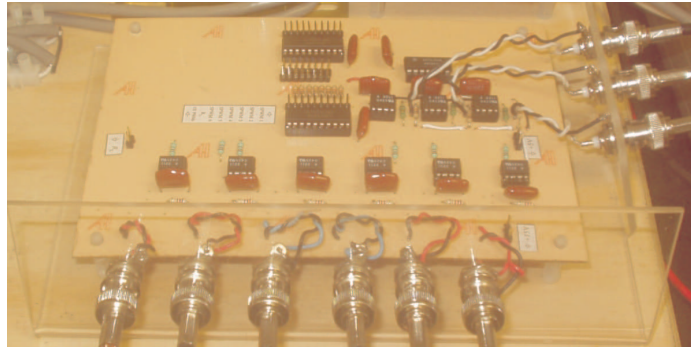


Figure 4.9 Picture of the control interface card.

An interface card is also designed to safely send the switching sequences, generated by the control law programmed in the DS1103 card, to the SKHI-22A drivers, where galvanic isolation is provided by means of optocouplers. In addition, this card protects the VSI against short circuit and power supply low voltage conditions. This protection is performed after interpretation of the three error signals coming out of the drivers SKHI-22A, namely, *Error 1*, *Error 2* and *Error 3*. Moreover, the control interface is able to interrupt the operation, by software, if conditions of over voltage or over current are detected by the sensors in the power stage. Figure 4.9 shows a picture of the control interface card, and Figure 4.10 shows the schematic of its electric circuit. The devices and parameters used in this card are listed in Table 4.4.

Control interface	
$R_{ic1}, R_{ic2}, R_{ic3}, R_{ic4}$	▷ 2.2 K Ω , 0.25 W
$C_{ic1}, C_{ic2}, C_{ic3}$	▷ 0.1 μ F
SN74LS540N, SN74LS541N	▷ buffers
HCPL-2211	▷ optocoupler
IC	▷ schematic representation for HCPL-2211 circuitry

Table 4.4 Devices and parameters of the control interface card.

The *operational manoeuvres circuits* are based on relays whose purposes are the pre-charge of capacitors, the connection and disconnection of the nonlinear load, as

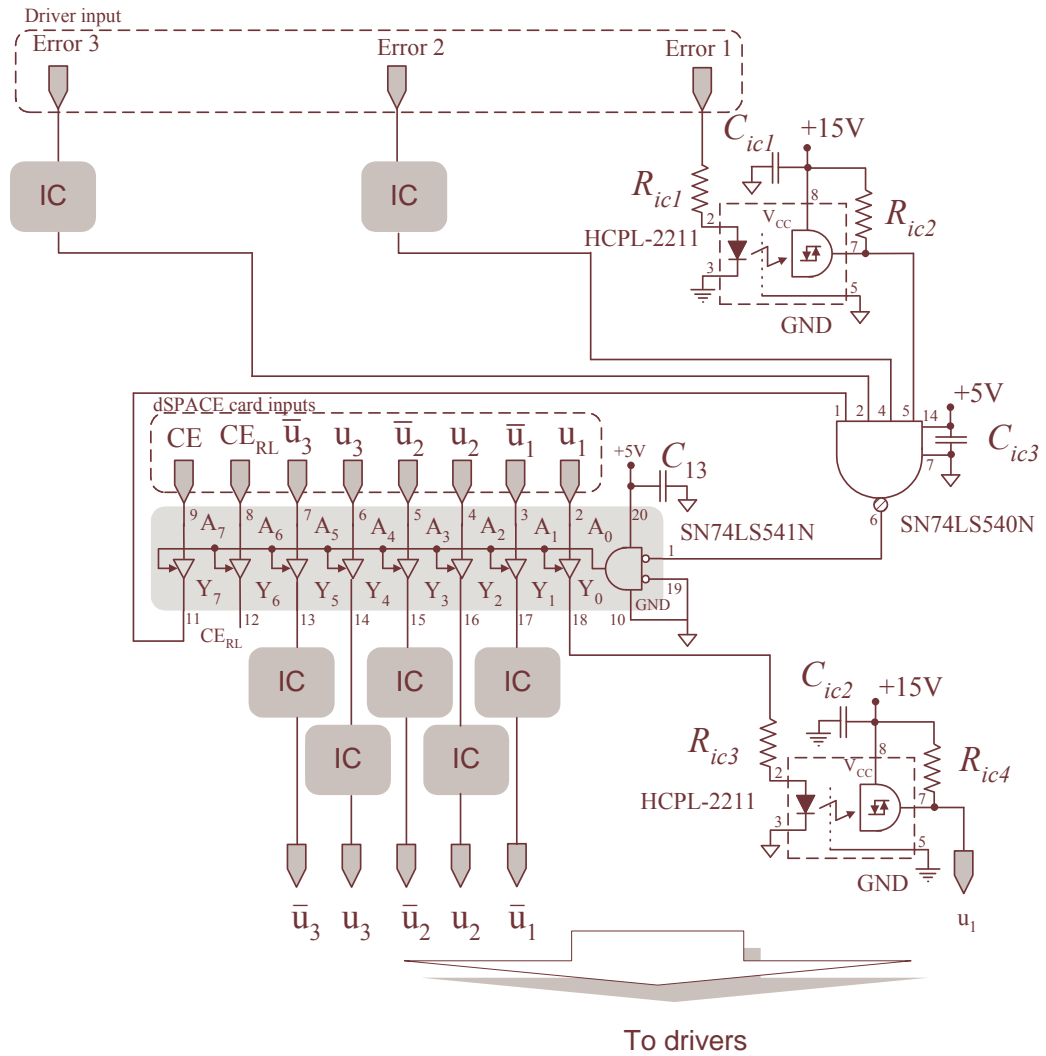


Figure 4.10 Schematic of the control interface card.

well as, the connection and disconnection of the active filter to the line. They are all necessary to guarantee a safe operation and protection of the active filter.

During the start up operation of the active filter a 50Ω at 160 W resistance is connected in series with the 5 mH inductance of the VSI by means of a relay, one resistance and one relay per phase. The objective of this operation is to precharge the capacitors to a certain level, and thus avoiding a higher peak of current at the control start up. Once the capacitors are charged, each 50Ω resistance is short-circuited with

another relay (one per phase). As previously mentioned, the control of these relays is done by the DS1103 card. The devices and parameters used in this card are listed in Table 4.5.

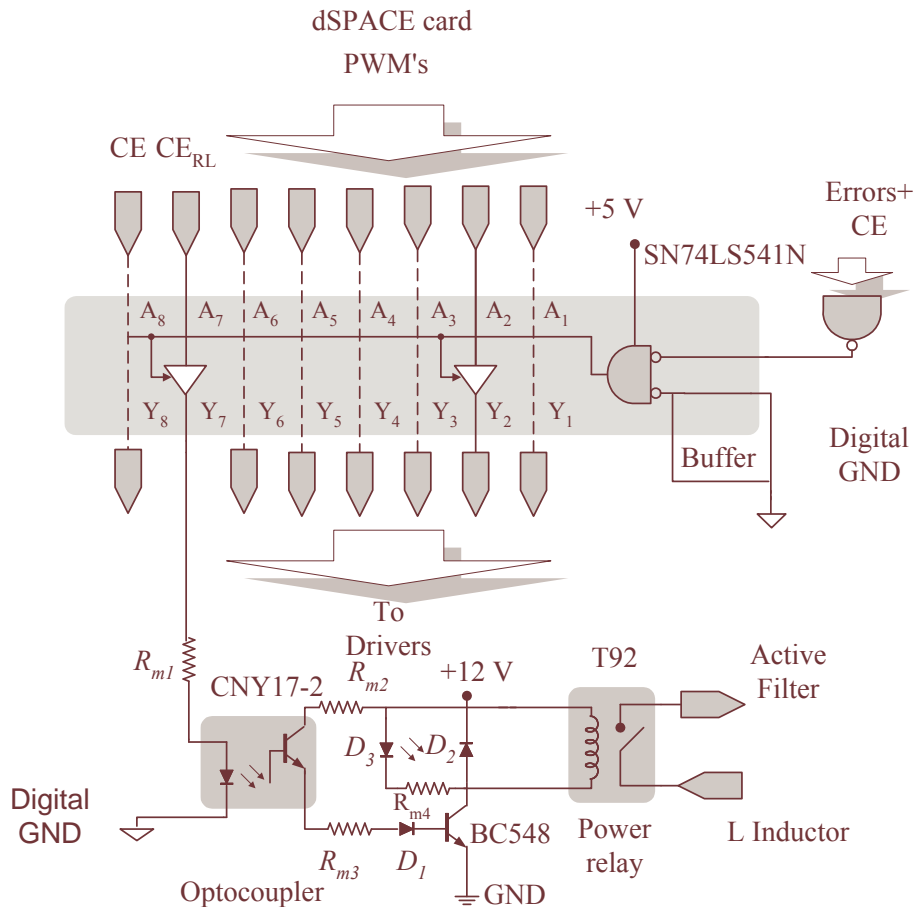


Figure 4.11 Electric circuit for the relays used in the operational manoeuvres.

Figure 4.11 shows the implemented circuitry for the relays used for the operational manoeuvres. The relays are activated by a chip enable signal CE_{RL} which is reinforced by the buffer SN74LS541N. The optocoupler CNY17-2 provides galvanic insulation between the buffer and the inductor of the power relay T92. The resistances R_1 work as current limiters for the CNY17-2 transistors. The 1N4937 diode D_1 restricts the current to flow only on the direction towards the CNY17-2 transistor. The diode D_2

Operational manoeuvres	
R_{m1}	▷ 330 Ω , 0.25 W
R_{m2}, R_{m4}	▷ 2.2 K Ω , 0.25 W
R_{m3}	▷ 220 K Ω , 0.25 W
T92	▷ power relay
D_1, D_2	▷ 1N4937 diode
D_3	▷ light emitter diode
BC548	▷ transistor
SN74LS541N	▷ buffer
CNY17-2	▷ optocoupler

Table 4.5 Devices and parameters of the control interface card.

deviates the inverse current produced by the bobbin of the power relay during its turn off process. The light emitter diode D_3 indicates the actual state of the power relay. Notice that, if the DS1103 control signal is a logic ON, then both transistors conduct activating the bobbin of the power relay, thus allowing the output current to flow, while for a logic OFF, they both are open.

4.3 Instrumentation stage

The *instrumentation stage* includes signal conditioning circuits for the current and voltage sensors, as well as voltage limiters. The three source currents are measured using hall effect CLN-25 current sensors. The three source voltages are measured using instrumentation transformers, while the dc voltages on the capacitors is obtained with voltage transducers LVP-25. Notice that, in these cases the galvanic isolation is provided by the same sensors. Signal conditioners and voltage limiters are implemented to try to fit the signals to the ranges allowed by the acquisition ports in the dSPACETMcard.

The implementation of the proposed controller requires the measurement of all three source current signals (i_{S1} , i_{S2} and i_{S3}), all three input voltages (v_{S1} , v_{S2} and v_{S3}) and the two capacitors voltages (v_{C1} and v_{C2}). The i_{S0} is not strictly necessary as it can be computed from $i_{S0} = i_{S1} + i_{S2} + i_{S3}$ as was remarked in Chapter 2. This section describes the signal conditioning electronics for current and voltage sensors. It is clear that, this circuits must provide a signal in an admissible range for the DS1103 card, as well as galvanic isolation between the power stage and the DS1103 card. In the case of the analog to digital (A/D) converter port in the DS1103, the allowed range for input signals is ± 10 V. Therefore, additional voltage limiters are introduced to restrict all analog signals to this range. The circuitry of such voltage limiters is also described here.

4.3.1 Source current sensor circuit

Figure 4.12(a) shows the electric circuit of the current sensor and its signal conditioner (one for each phase). As observed in this diagram, the closed-loop hall effect sensor provides a current signal proportional to the source current signal. This output current signal is then transformed to a voltage signal, by means of a current-to-voltage circuit implemented with the operational amplifier TL082. The transfer function from the k -th source current i_{Sk} to the corresponding delivered voltage v_{iSk} is given by

$$v_{iSk} = 1 \times 10^{-3} \left(\frac{R_{cs2}R_{cs3}}{R_{cs1}} \right) i_{Sk} \quad , \quad k \in \{1, 2, 3\}$$

A picture of the implemented circuitry is provided in Fig. 4.12(b). Table 4.6 shows the devices and parameters used to build this circuitry.

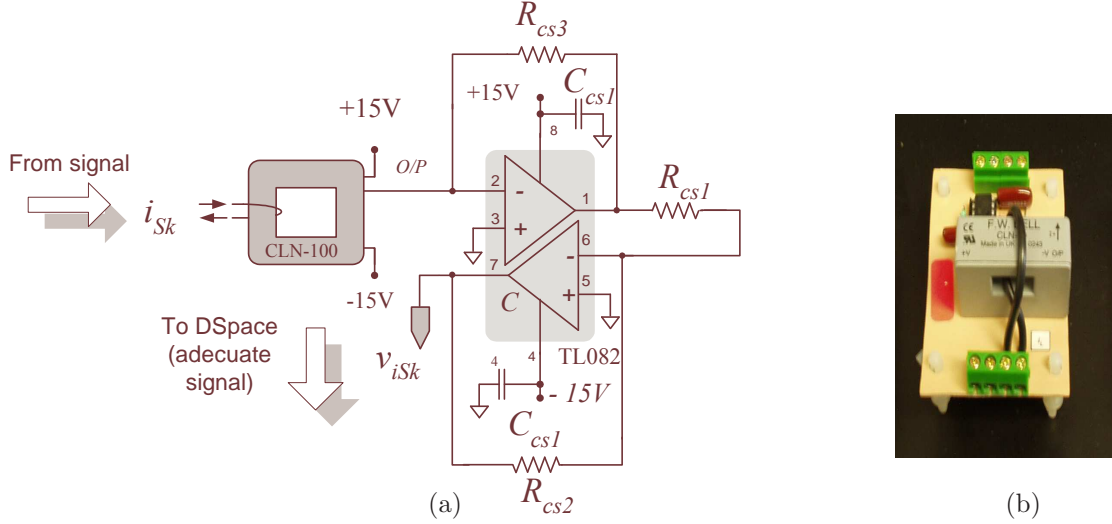


Figure 4.12 (a) Schematic of the current sensor and its signal conditioner, and (b) picture of the physical implementation.

4.3.2 Input voltage sensor circuit

The electric circuit and an picture of the implemented circuitry are shown in Fig. 4.13(a) and Fig. 4.13(b), respectively. In this diagram, the transformer is used to reduce the input voltage with a rate 1/10, then the resulting voltage is adequate by the operational amplifiers within TL082.

The transfer function of the k -th source voltage v_{Sk} to the corresponding delivered voltage v_{vSk} is given by the expression.

$$v_{vSk} = 1 \times 10^{-3} \left(\frac{R_{vs2} R_{vs3}}{R_{vs1} R_{vs4}} \right) v_{Sk} \quad , \quad k \in \{1, 2, 3\}$$

Table 4.7 shows the devices and parameters used to implement the input voltage sensor circuit.

Current sensor circuit	
R_{cs1}, R_{cs2}	▷ 5 kΩ, 0.25 W
R_{cs3}	▷ 10 kΩ, 0.25 W
C_{cs1}	▷ 0.1 μF, 50 V
CLN-100	▷ closed-loop hall effect current sensor
TL082	▷ encapsulated with two operational amplifiers
i_{Sk}	▷ k-th source current, $k \in \{1, 2, 3\}$
v_{iSk}	▷ voltage delivered by the k-th signal conditioner circuit, $k \in \{1, 2, 3\}$

Table 4.6 Devices and parameters used in the current sensor circuit.

Input voltage sensor circuit	
$R_{vs1}, R_{vs2}, R_{vs3}$	▷ 10 kΩ, 0.25 W
C_{vs1}, C_{vs2}	▷ 0.1 μF, 50 V
TL082	▷ dual operational amplifier
v_{Sk}	▷ k-th source voltage, $k \in \{1, 2, 3\}$
v_{vSk}	▷ voltage delivered by the k-th signal conditioner, $k \in \{1, 2, 3\}$

Table 4.7 Devices and parameters used in the input voltage sensor circuit.

4.3.3 Capacitor voltage sensor circuit

Figure 4.14(a) shows the implemented electric circuitry for the capacitor voltage sensor. In this diagram the LV25-P voltage transducer produces a current signal proportional to the source voltage signal. The current signal delivered by the transducer is then converted to a voltage signal with the aid of a current-to-voltage circuit built with an operational amplifier TL082. The transfer function from the k-th capacitor voltage v_{Ck} to the corresponding voltage delivered by the sensor circuitry v_{vCk} is given by

$$v_{vCk} = 0.4 \left(\frac{R_{vc2}R_{vc3}}{R_{vc1}} \right) v_{Ck} \quad , \quad k \in \{1, 2\}$$

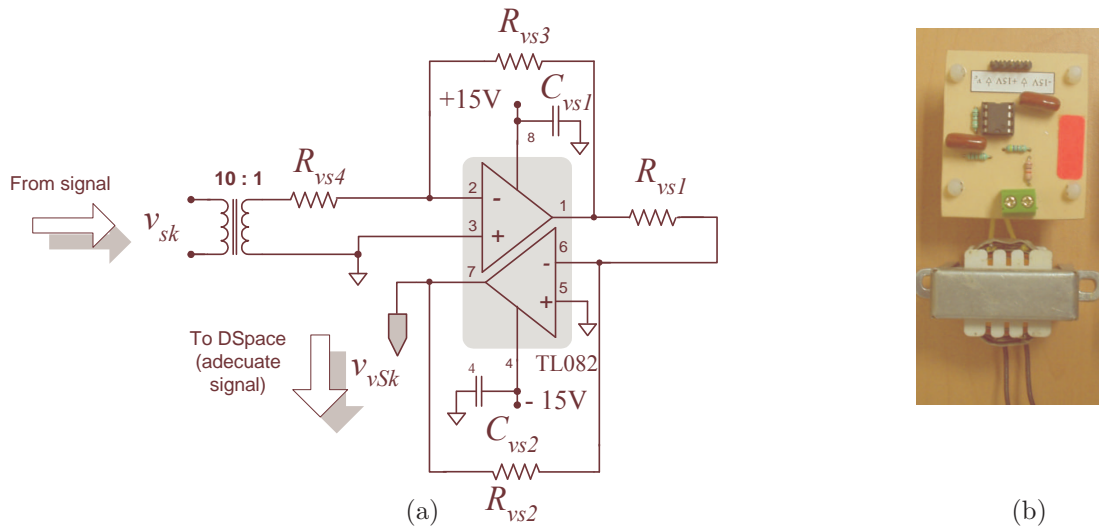


Figure 4.13 (a) Electric circuit of the input voltage sensor, and (b) picture of the physical implementation.

Figure 4.14(b) shows a picture of the implemented circuitry for the capacitor voltage sensor. Table 4.8 shows the devices and parameters used to implement this voltage sensor.

4.3.4 Voltage limiter interface card

The previous sensors circuits have been developed to deliver a voltage in the DS1103 admissible range (± 10) during normal operation, that is, in the steady state. Evidently, a relatively small margin of security has been considered which allows only small transients. However, to effectively protect the DS1103 card, a voltage limiter interface card is required to restrict the voltage signals, delivered by the sensor circuits, to the range ± 10 before sending them to the DS1103 A/D input ports.

Figure 4.15(a) and Fig. 4.15(b) show the electric circuitry and a picture of this voltage limiter card, respectively. In this diagram is observed that, the TL082 works as a noninverting voltage follower, the resistance R_{L1} limits the current through the TL082, while the zener diodes D_{L1} and D_{L2} keep the output voltage v_{ADin} in the safe range (± 10). Table 4.9 shows the devices and parameters used to build this card.

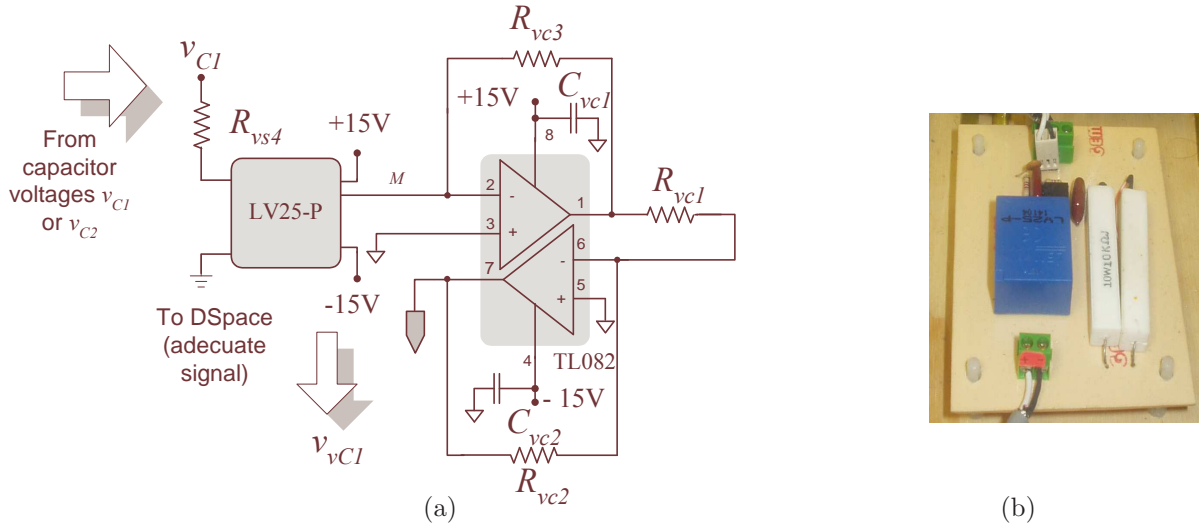


Figure 4.14 (a) Schematic of the capacitor voltage sensor, and (b) picture of the physical implementation.

Capacitor voltage sensor circuit		
R_{vc1}	▷	2.2 K Ω , 0.25 W
R_{vc2}	▷	170 Ω , 0.25 W
R_{vc3}	▷	4.7 K Ω , 0.25 W
R_{vc4}	▷	20 K Ω , 10 W
C_{vs1}, C_{vs2}	▷	0.1 μ F, 50 V
TL082	▷	dual operational amplifier
LV25-P	▷	voltage transducer
v_{Ck}	▷	k-th capacitor voltage, $k \in \{1, 2\}$
v_{vCk}	▷	voltage delivered by the k-th capacitor voltage sensor, $k \in \{1, 2\}$

Table 4.8 Devices and parameters used in the capacitor voltage sensor circuit.

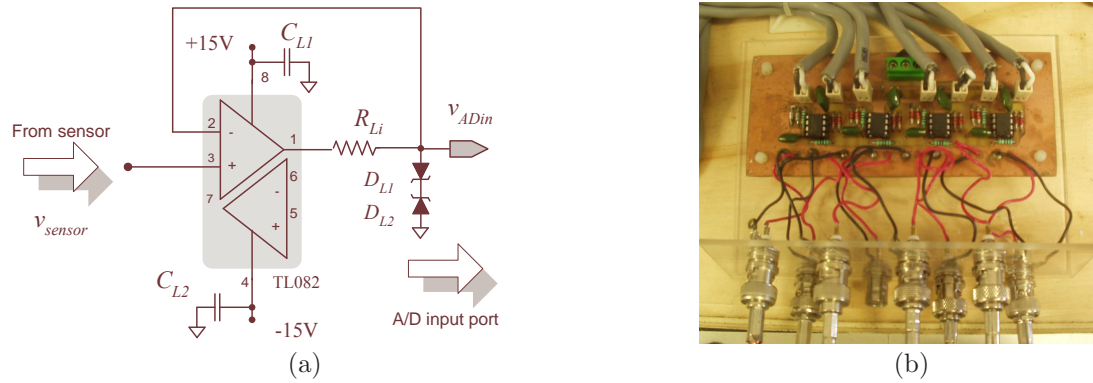


Figure 4.15 (a) Electric circuit of the voltage limiter, and (b) picture of the physical implementation.

Voltage limiter interface card	
R_{L1}	▷ 100 Ω , 0.25 W
C_{L1}, C_{L2}	▷ 0.1 μF , 50 V
D_{L1}, D_{L2}	▷ 12 V zener diodes;
TL082	▷ dual operational amplifier
v_{sensor}	▷ voltage delivered by a sensor circuit
v_{ADin}	▷ voltage delivered to the DS1103 A/D input port

Table 4.9 Devices and parameters used in the voltage limiter interface card.

5. RESULTS

5.1 Introduction

The proposed controller was tested by means of a 2 kVA three-phase four-wire shunt active filter whose design is explained in Chapter 4. As previously mentioned, the prototype has the following parameters: $L = 5$ mH, $C = 1100$ μ F, $2Vd = 340$ V and an input voltage amplitude of 110 V RMS with a fundamental frequency of $f_0 = 60$ Hz ($\omega_0=377$ r\s). The load is composed of a three-phase diode rectifier with an associated load resistance of 75 Ω , in addition, a single-phase diode-bridge rectifier is connected between a phase and the neutral line to produce the homopolar current component. A capacitor of 470 μ F and a load resistance which is changing between 350 Ω and 175 Ω are connected to the DC-side of this single-phase rectifier. The switching frequency f_{sw} is set to 18 kHz. The control stage, as mentioned before, is implemented by means of a DS1103, where the sampling rate is fixed to 14.28 kHz.

As shown in Chapter 3 a bank of resonant filters (3.19) is necessary to compensate the harmonic disturbance. However, the resonant filters exhibit an infinite gain at the resonance frequency, which may entail instability problems. To alleviate this issue, it is proposed to use band-pass filters (BPF) in the place of the resonant filters, thus guaranteeing a safer operation. Recall that, BPFs have limited gain due a damping term introduced in the denominator of the transfer function as shown below

$$\hat{\phi}_{k,\alpha\beta} = \frac{2sk\omega_0 A_k/Q_k}{s^2 + sk\omega_0/Q_k + k^2\omega_0^2} \tilde{\mathbf{i}}_{S\alpha\beta} \quad , \quad k \in \mathcal{H} \quad (5.1)$$

where A_k and Q_k are positive design parameters representing the desired gain and the quality factor of the k-th BPF, respectively. The bank of BPFs includes filters tuned at 1st, 3rd, 5th, 7th and 9th harmonic of the fundamental ω_0 , which are the harmonic components considered for compensation. Notice that, the original gain γ_k

in the resonant filters has been replaced by A_k/Q_k . The design parameters of the controller are selected as follows: $A_1 = 3, Q_1 = 7, A_3 = 40, Q_3 = 10, A_5 = 35, Q_5 = 5.5, A_7 = 10, Q_7 = 4$.

The tuning of the remaining control parameters is performed following the next approximations. First, notice that, in this system the fastest dynamics is the current loop dynamics, formed by 3.1 in closed loop with the controller 3.18, which yields

$$(Ls\mathbf{I}_2 + \mathbf{K}_1)\tilde{\mathbf{i}}_{S\alpha\beta} = \tilde{\boldsymbol{\phi}}_{k,\alpha\beta} \quad (5.2)$$

where s represents the laplace complex variable. In this case, the design matrix \mathbf{K}_1 used to introduce the required damping can be set as $\mathbf{K}_1 = k_1 \cdot \mathbf{I}_2$ where k_1 is a proportional gain and \mathbf{I}_2 represents the 2×2 identity matrix. Its bandwidth, according (5.2) is given by k_1/L should be at most 1/10 to 1/14 of the sampling frequency $2\pi f_s$. Therefore, the gain k_1 can be approximated by $k_1 \cong \pi L f_s / 7$, which according to the prototype parameters gives $k_1 \cong 18.85$. However, better results have been observed for a $k_1 = 15$.

In the outer loop case, the capacitor dynamics (3.2) in closed loop with the controller (3.21) yields the following third order system

$$C\dot{\tilde{z}}_4 = -k_{p1}\chi_4 - k_{i1}\xi + c_2 - \frac{2\tilde{z}_4}{R} \quad (5.3)$$

$$\dot{\xi} = \tilde{z}_4 \quad (5.4)$$

$$\tau_1\dot{\chi}_4 = -\chi_4 + \tilde{z}_4 \quad (5.5)$$

Usually, τ_1 is selected is such a way that, $1/\tau_1 > 2w_0$, where w_0 represents the fundamental of the line voltage. Since $\tau_1 \ll 1$ then, its effect can be neglected from the previous control expression, therefore, the characteristic polynomial can be reduced to

$$\left(s^2 + \left(\frac{k_{p1}}{C} + \frac{2}{RC} \right) s + \frac{k_{i1}}{C} \right) \tilde{z}_4 = 0 \quad (5.6)$$

Notice that, due to the ripple on the dc voltage at twice the supply frequency during unbalanced operation, the voltage loop bandwidth should be limited to approximately 10 Hz (cutoff frequency) in order to avoid possible amplification of the second harmonic in the line current reference. In the present work the parameters $k_{p1} = 10.965$ and $k_{i1} = 18.06$ have been selected.

Notice that, in order to fulfill with the decoupling assumption, the bandwidth of voltage loop system should be at most 1/10 of the current dynamics bandwidth, which is largely fulfilled for the selected parameters.

Similar to the inner loop controller of subsystem A, the bank of resonant filters to build \hat{v} in (3.46) in the homopolar compensation loop are replaced by a bank of BPFs with transfer function given by

$$\hat{v} = \frac{sm\omega_0\mathcal{A}_m/\mathcal{O}_m}{s^2 + sm\omega_0/\mathcal{O}_m + m^2\omega_0^2}i_{S\gamma} \quad , \quad m \in \mathcal{H}_2 \quad (5.7)$$

where \mathcal{A}_m and \mathcal{O}_m are positive design parameters representing the desired gain and the quality factor of the m-th BPF, respectively. The bank of BPFs includes filters tuned at 1st, 3rd, 5th, 7th and 9th harmonics of the fundamental ω_0 , which are the harmonic components considered for compensation. The original gain λ_m in the resonant filters has been replaced by $\mathcal{A}_m/\mathcal{O}_m$. The design parameters of the controller were selected as follows: $\mathcal{A}_1 = 3, \mathcal{O}_1 = 7, \mathcal{A}_3 = 40, \mathcal{O}_3 = 10, \mathcal{A}_5 = 35, \mathcal{O}_5 = 5.5, \mathcal{A}_7 = 10, \mathcal{O}_7 = 4$.

The rest of the controller gains for the homopolar compensation loop (3.25) and (3.26) have been selected as $k_2 = 60$ and $k_{p2} = 0.2$.

Different tests have been carried out to exhibit the performance of this solution and to show the correct fulfillment of the main objectives, namely, tracking, homopolar compensation, regulation and balance. These results, shown in the following sections, include steady state responses, transient responses due to changes in the load, and comparison with respect to the PI controller.

5.2 Tracking results: harmonic disturbance and reactive power compensation

As pointed out in Section 2.2.1, the tracking objective consist in forcing $i_{S\alpha\beta}(t)$ to track a reference signal proportional to the line voltage $v_{S\alpha\beta}(t)$, so that, from the source terminals viewpoint, the same apparent resistance is observed in all phases.

The Fig. 5.1 shows (from top to bottom) the steady state response of the input voltages of all three phases (the phase number is indicated below each plot). Notice

that, the input voltages are almost sinusoidal signals that have been slightly distorted, and thus, they contain some higher order harmonic components. This is independent of the load current distortion. The next three signal plots represent the three compensated line (or source) currents, after the proposed control is enabled. Notice that, as expected, the line currents get a form proportional and in phase to the corresponding line voltages, that is, tracking of the line currents over the reference (scaled input voltage) is reached. Notice also that, the neutral line current, presented in the last signal plot in the bottom, almost reaches zero. The last confirms that the homopolar (neutral) current compensation objective is fulfilled.

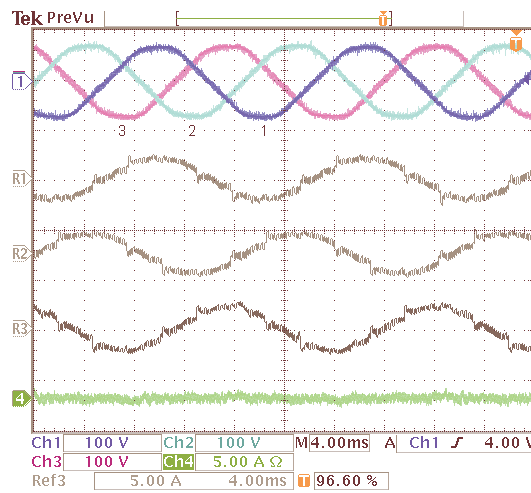


Figure 5.1 (**Top plot**) Steady state responses of the active filter under the overall proposed solution. Three line voltage (250 V/div), (**four last plots**) three line current (10 A/div) and homopolar (neutral) current (5A/div).

Figure 5.2 shows (from top to bottom) the steady state response of the line voltages of all three phases. The four last plots show the load currents in all three phases where the nonlinear and unbalance condition is reflected, plus the existence of a considerable homopolar component of the load current.

Figure 5.3 shows (from top to bottom) the frequency spectrum of the voltage line (only phase v_{S3} is shown which is the most distorted phase), the corresponding load current, and the corresponding compensated line current. Notice that, in the proposed controller, the third, fifth, seventh and ninth harmonic components have

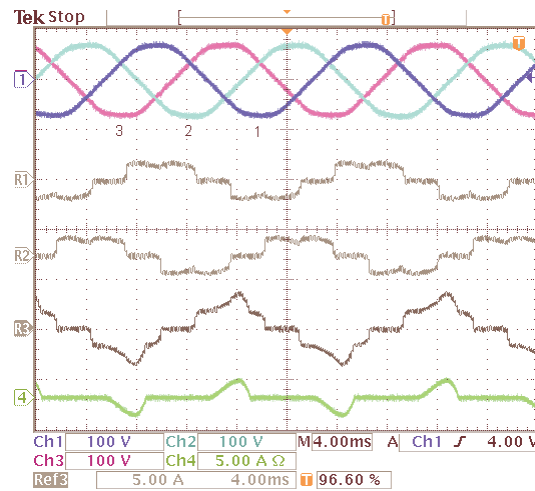


Figure 5.2 (**Top plot**) Three line voltages (250 V/div), (**four last plots**) three load currents (10 A/div) and homopolar component of the load current (5A/div).

been reduced. Table 5.1 shows the percent of each harmonic component of both the load current and the compensated line current. Notice that, the THD reached with the proposed controller is 9.5 %, while that of the load current is 30.98%.

To compute the THD the following expression has been used (see [29])

$$\%THD = 100 \times \frac{(\sum_{h=2}^{\infty} x_h^2)^{\frac{1}{2}}}{x_1}$$

where x_h represent the RMS value of the harmonic of order h , and x_1 represent the RMS value of the fundamental component.

Harmonic	3rd(%)	5th(%)	7th(%)	9th(%)	THD(%)
Load current	25.12	15.85	6.31	3.98	30.63
Compensated line current	2.51	6.31	2.51	1	7.3

Table 5.1 The THD reached with the proposed controller in comparison with the THD of the load current.

Figures 5.4, 5.5 and 5.6 show (from top to bottom) the steady state response of line

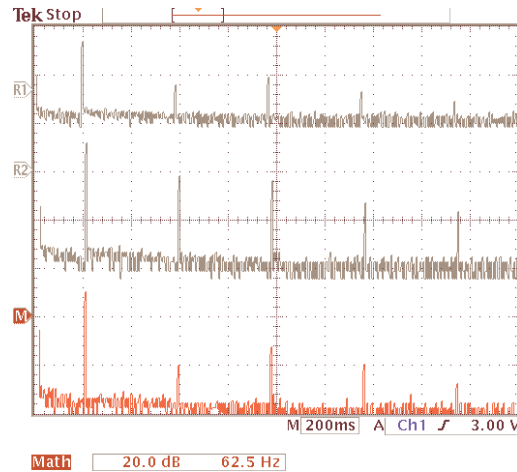


Figure 5.3 **(Top)** Spectra of line voltage v_{S3} (20 dB/div). **(reference bottom plot)** Spectra of line current i_{S3} (20 dB/div). **(red bottom plot)** Spectra of compensated line current i_{S3} (20 dB/div).

voltage, compensated line current, load current and injected current (for one phase only). Fig. 5.4 shows the responses of PI control scheme (the same PI controller used for regulation voltage of VSI plus a proportional term with a high gain is used for the current compensation). Notice that, a poor current tracking is observed, that is, the compensated line current has considerable distortion, and thus, its shape does not fit that of the line voltage. Figure 5.5 shows the response of the proposed controller when the homopolar compensation part has been disabled, i.e., only the harmonic compensation scheme based on the resonant filters is considered. Finally, Fig. 5.6 shows the responses of the overall proposed controller. Notice that, although the tracking in Fig. 5.5 is better than in the conventional controller shown in Fig. 5.4, the tracking can be considerably improved if efforts are carried out to compensate the homopolar component simultaneously.

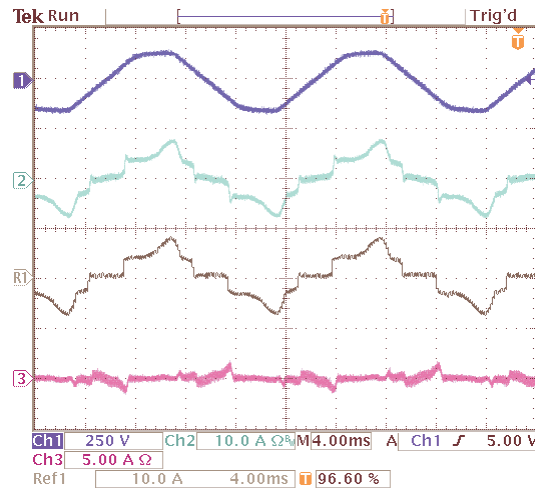


Figure 5.4 (From top to bottom) Steady state responses of the active filter under the conventional controller: line voltage (250 V/div), line current (10 A/div), load current (10 A/div) and (inverted) injected current (10 A/div).

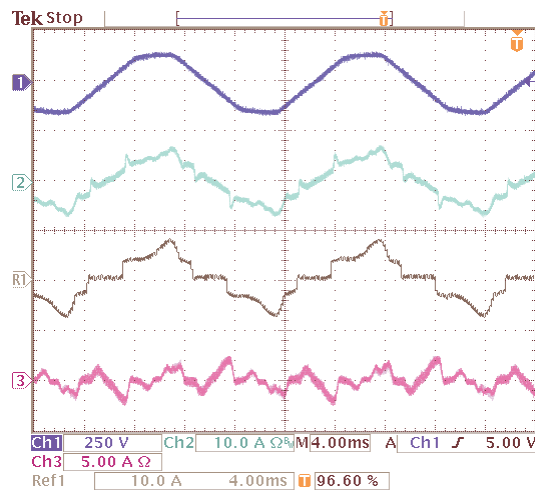


Figure 5.5 (From top to bottom) Steady state responses of the active filter under the proposed controller with the homopolar compensation part disable: line voltage (250 V/div), line current (10 A/div), load current (10 A/div) and (inverted) injected current (10 A/div).

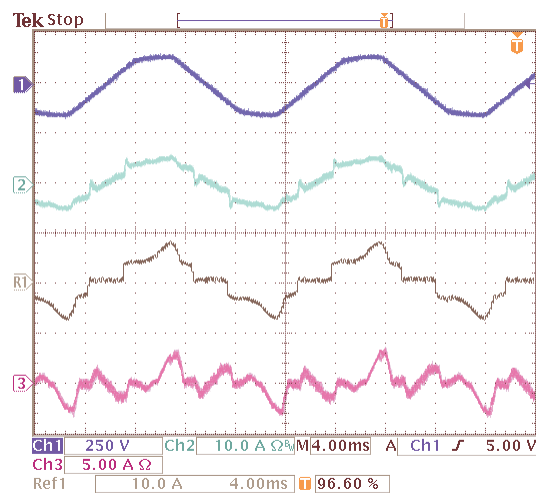


Figure 5.6 (From top to bottom) Steady state responses of the active filter under the overall proposed controller: line voltage (250 V/div), line current (10 A/div), load current (10 A/div) and (inverted) injected current (10 A/div).

5.3 Homopolar current component compensation

As previously mentioned in Section 2.2.2, the proposed controller is able to cancel the current flowing through the neutral conductor due to the homopolar component of the load current. Figure 5.7 shows (from top to bottom) the compensated neutral line current i_{S0} , the homopolar component of the load current i_{L0} and the injected neutral current i_0 under the PI control scheme proposed by the regulation objective. Notice that, the injected current i_0 does not provides any improvement, and thus the neutral line current has a magnitude similar to that of the homopolar component of the load current, in fact, only the harmonics due to switching are aggregated as noise, in other words, the homopolar compensation objective cannot be fulfilled. Figure 5.8 shows the same signals (as in previous figure) for the proposed controller, when the homopolar compensation part has been disabled. Notice that, in case that no provision is made for the current homopolar compensation, and even if the harmonic compensation part is trying to guarantee a good tracking of the line currents, the final effect is a considerable increase in the neutral line current flowing to the source. Finally, Fig. 5.9 shows, for the proposed controller, (as in the two previous figures) the compensated neutral line current i_{S0} , the homopolar component of the load current i_{L0} , and the injected neutral current i_0 . Notice that, i_{S0} reaches an amplitude close to zero as expected, and additionally, the tracking of the line current towards the shape of the line voltage is considerably improved.

Figure 5.10 shows the steady state response of the load current homopolar component and its frequency spectrum. Figure 5.11 shows the compensated neutral line current for PI controller used in the regulation objective. Notice that, the harmonic contents of this current and that of the load current homopolar component is very similar. Figure 5.12 shows also the compensated neutral line current for the proposed controller with the homopolar compensation part disabled. It is observed here that the distortion of this current is increased, which is reflected in the increment on harmonic components 5th and 9th. The response of the complete proposed solution is shown in Fig. 5.13, where it is observed that the homopolar compensation objective is reached, that is, the compensated neutral line current is considerably reduced, and thus its harmonic contents is also reduced.

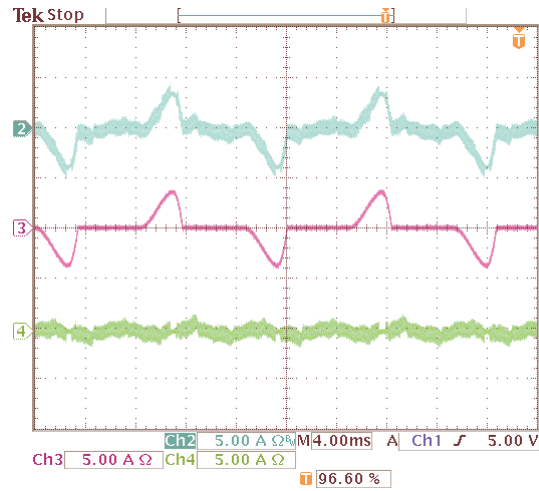


Figure 5.7 Responses under the conventional controller (**from top to bottom**): compensated neutral line current i_{S0} (5 A/div), homopolar component of the load current i_{L0} (5 A/div), and neutral injected current i_0 (5 A/div).

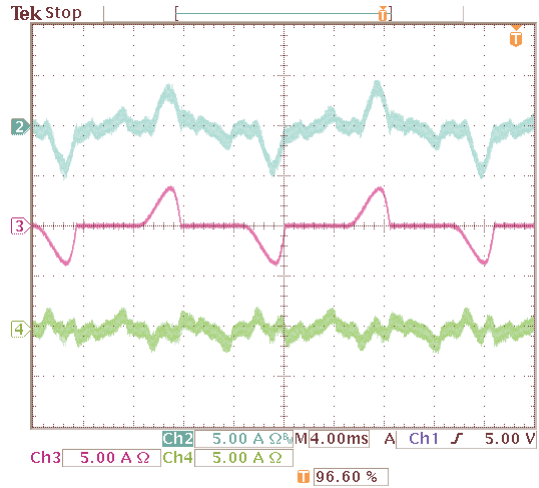


Figure 5.8 Responses under the proposed controller with the homopolar compensation part disabled (**from top to bottom**): compensated neutral line current i_{S0} (5 A/div), homopolar component of the load current i_{L0} (5 A/div), and neutral injected current i_0 (5 A/div).

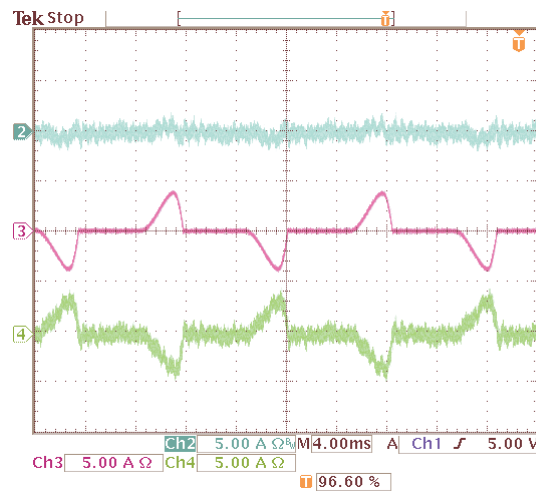


Figure 5.9 Responses under the overall proposed controller (**from top to bottom**): compensated neutral line current i_{S0} (5 A/div), homopolar component of the load current i_{L0} (5 A/div), and neutral injected current i_0 (5 A/div).

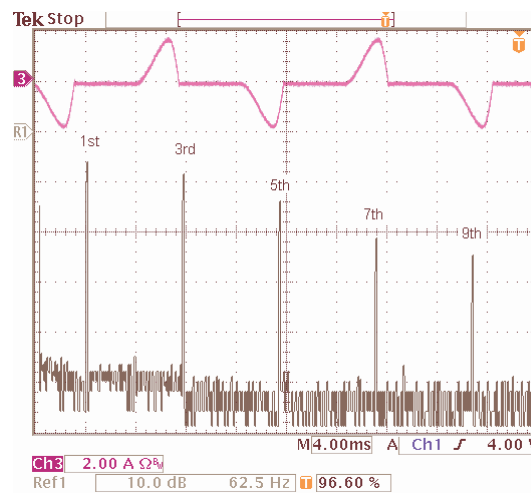


Figure 5.10 (**Top**) Load current homopolar component i_{L0} (2 A/div) and (**bottom**) its frequency spectrum (10 dB/div).

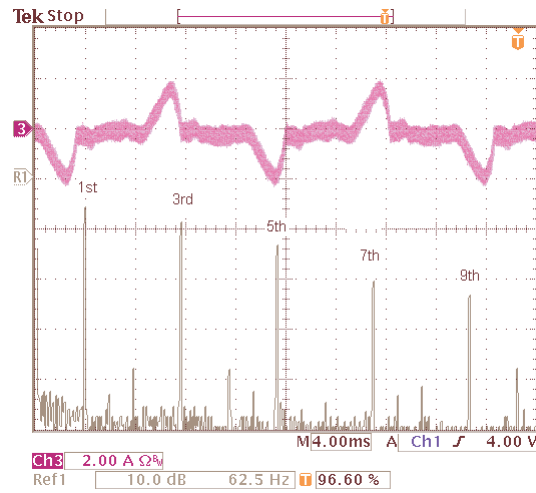


Figure 5.11 (Top) Compensated neutral line current i_{S0} (2 A/div) and (bottom) its frequency spectrum (10 dB/div) with conventional controller.

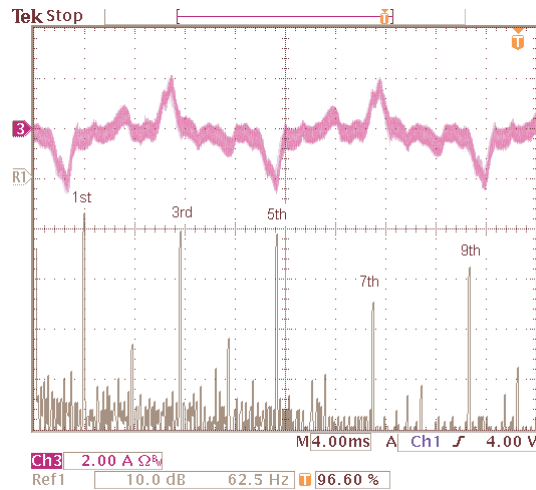


Figure 5.12 (Top) Compensated neutral line current i_{S0} (2 A/div) and (bottom) its frequency spectrum (10 dB/div) with the proposed controller disabling the homopolar compensation part.

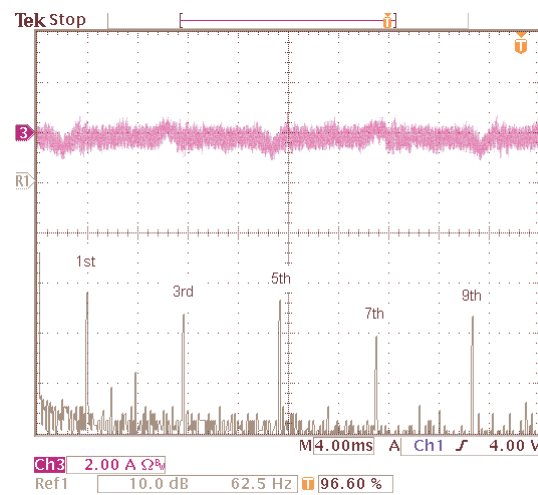


Figure 5.13 (Top) Compensated neutral line current i_{S0} (2 A/div) and (bottom) its frequency spectrum (10 dB/div) with the overall proposed controller.

Table 5.2 presents the percent of each harmonic component of the load current homopolar component, and the compensated neutral line currents under the different control cases, namely, PI controller, proposed controller with homopolar compensation part disabled, and overall proposed controller.

Current	1st(%)	3rd(%)	5th(%)	7th(%)	9th(%)
i_{L0}	100.00	89.12	63.00	42.10	33.49
i_{S0} PI	100.00	89.12	66.80	44.60	35.48
i_{S0} disabling homop.	94.40	79.43	74.98	35.48	50.11
i_{S0} proposed	31.81	31.62	35.48	25.11	31.00

Table 5.2 Comparison of the percentage of the different harmonic components of the compensated neutral line current under the different control schemes.

5.4 Voltage regulation and voltage balance results

To guarantee a correct operation and prevent damage to the active filter, it was stated in Sections 2.2.3 and 2.2.4 that, the sum of voltages x_4 should be forced to take a constant value reference $2V_d = 340$ V, while the difference of capacitor voltages x_5 should be zeroed, at least in the average. It was stated as well that, these objectives are equivalent to demand that both capacitors reach, simultaneously, the same constant reference V_d . Figure 5.14 shows the transient response of the sum of voltages x_4 , the difference of voltages x_5 and the scaled conductance $gv_{S,RMS}^2$ under the proposed controller. The transient is due to a load change in the single-phase diode-bridge rectifier from 175Ω to 350Ω and back. Notice that, after a relatively small transient the sum of voltage x_4 is maintained in the desired constant value $2V_d = 340$ V, while x_5 is maintained bounded and very close to zero.

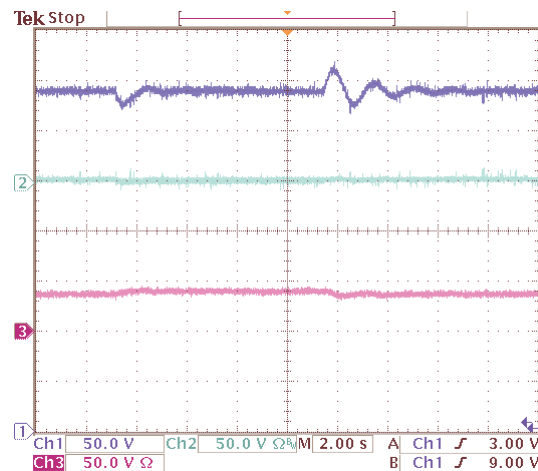


Figure 5.14 (From top to bottom) Sum of the capacitor voltages x_4 (50 V/div), difference of the capacitor voltages x_5 (50 V/div), and scaled apparent conductance $gv_{S,RMS}^2$ (500 W/div).

5.5 Transient Response

The transient response of the compensated neutral line current is shown in Fig. 5.15 for a load change from $350\ \Omega$ to $175\ \Omega$, and from $175\ \Omega$ to $350\ \Omega$ in Fig. 5.16. Notice that, the homopolar compensation objective is fulfilled even after a load change condition.

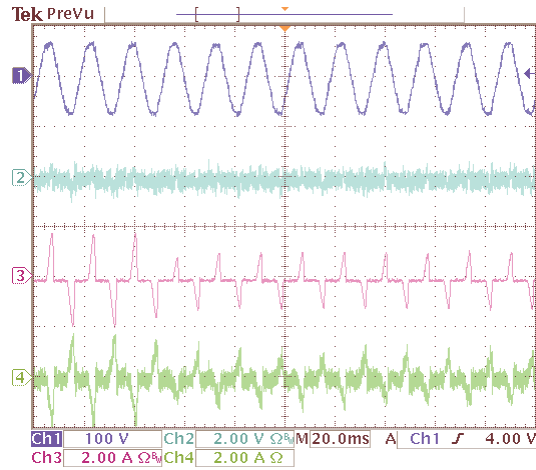


Figure 5.15 Transient responses of the active filter under a load change from $350\ \Omega$ to $175\ \Omega$ (from top to bottom): line voltage (100 V/div), compensated neutral line current i_{S0} (2 A/div), homopolar component of the load current i_{L0} (2 A/div), and injected neutral current i_0 (2 A/div).

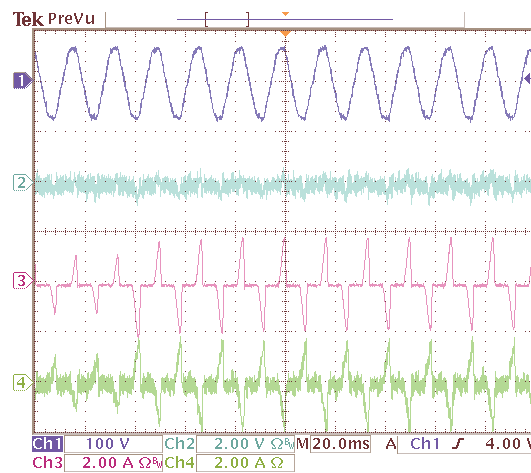


Figure 5.16 Transient responses of the active filter under a load change from 175Ω to 350Ω (**from top to bottom**): line voltage (100 V/div), compensated neutral line current i_{S0} (2 A/div), homopolar component of the load current i_{L0} (2 A/div), and injected neutral current i_0 (2 A/div).

6. CONCLUSIONS

This thesis work presented a model-based controller for a three-phase four-wire shunt active filter which uses a three-leg split capacitor topology to implement the VSI. This system represents a very interesting solution in distribution systems where loads are connected between a phase and the neutral line, with the neutral line shared by all phases. The last is based on the fact that this topology provides an alternative path for the flowing of the homopolar component of the load current, and thus enabling the compensation by an adequate controller. The proposed controller was aimed to compensate reactive power and harmonic distortion in the general case of distorted and unbalanced source voltages and load currents, including distorting loads connected between a phase and the neutral line. In addition, the controller was able to compensate the homopolar component of the load current without modifying the actual topology. In other words, the current flowing to the source via the neutral line was considerably reduced.

The solution presented in this work was based on the use of the γ -component of the control, voltages and currents. It was shown that this control γ -coordinate, usually neglected in many control algorithms, was the crucial element to allow both compensation of the homopolar current and balance of the capacitors voltages. The controller presented here was obtained following adaptive techniques which gave, in principle, a stable and robust controller, whose structure is very close to that of the conventional controller with some additional and necessary modifications. It has also been shown in this work that, the direct application of the conventional controller used in a three-phase three-wire system, without modifications, was not able to guarantee control over the homopolar component, an in fact, it may even contribute to increase such a neutral current.

To experimentally prove the proposed controller, a three-phase four-wire shunt active filter prototype was built. The power stage of the active filter was based on a commercial three-phase VSI, where the middle point of the bank of capacitors on the dc side was made accessible. The unbalanced load consisted of a three-phase diode rectifier feeding a resistor, plus single-phase diode-bridge rectifier connected in between one phase and neutral to produce unbalance and homopolar current flowing to through the neutral wire. For the instrumentation of the inverter prototype, sensors, signal conditioners, voltage limiters and a control interface have been implemented as well. The experimental results with the proposed controller exhibited the fulfillment of the proposed objectives. First, the compensation of the homopolar component of the load current was guaranteed, out of which, it was observed a considerable reduction of the current in the neutral wire. Second, the capacitors voltages balance was satisfied at least in the average. A very important remark here was that, it is not possible to completely zero the difference between the capacitors voltages, and thus a certain ripple

The future research will be focused on the introduction of repetitive schemes ([30] and [31]) on the controller to allow harmonic compensation, roughly speaking, the idea is to replace the whole bank of resonators by a simpler repetitive scheme. This will reduce the computational load, while preserving, and even improving, the performance. All the prototype will be enclosed in a cabinet where the dSPACE card will be substituted by a reduced cost digital signal processor (DSP) card. Perhaps a fixed point DSP based card would be the most interesting from the cost viewpoint, in addition all signal conditioners and voltage limiters will be included in the same card, which will reduce the noise in signals and thus improve the performance. The commercial VSI will be substituted by a laboratory assembled VSI.

BIBLIOGRAPHY

- [1] P.N. Enjeti, W. Shireen, P. Packebush, and I. J. Pitel. Analysis and design of a new active power filter to cancel neutral current harmonics in three-phase four wire electric distribution systems. *IEEE Trans. on Ind. Appl.*, 30:1565–1572, 1994.
- [2] C.A. Quinn and N. Mohan. Active filtering of harmonic currents in three-phase, four-wire systems with three-phase and single-phase nonlinear loads. *Int. Power Elec. Conf. : IPEC '92*, pages 829–836, 1992.
- [3] A. Chaghi, A. Guettafi, P. , and A. Benoudjit. Four-legged active power filter compensation for a utility distribution system. *Journal of Electrical Engineering*, 55:31–35, 2004.
- [4] J. Paschal. *Practical Guide to Power Factor Correction and Harmonics...and Your Electric Bill*. EC and M Books, ISBN 0872887115, 2001.
- [5] C.A. Quinn, N. Mohan, and H. Mehta. A four-wire, current controlled converter provides harmonic neutralization in three-phase, four-wire systems. *Int. Power Elec. Conf. : IPEC '93*, pages 841–846, 1993.
- [6] G. Escobar, A.A. Valdez, and Torres-Olguin R.E. A novel model-based controller for a three-phase four-wire shunt active filter. *Proc. IEEE Pow. Elec. Spec. Conf. (PESC)*, pages 119–126, 2006.
- [7] R. Arthur and R.A. Shanahan. Neutral currents in three phase wye systems. *Power Systems Engineering Data published by Square D*, 1996.
- [8] M. Lowenstein and M. McGranaghan. Ask the experts. *available in website <http://www.ecmweb.com/>*, 2006.

- [9] G. Dinykel and R. Gretsche. Kompensator für Oberschwingungen und Blindleistung.
- [10] G. Superti-Furga, E. Tironi, and G. Ubezio. General purpose low-voltage power conditioning equipment. In *Int. Power Elec. Conf. : IPEC '95*, pages 400–405, Yokohama, Japan, 1995.
- [11] M. Aredes, J. Häfner, and K. Heumann. A three-phase four-wire shunt active filter using six IGBT's. In *Eur. Conf. Power Elec. Conf. : EPEC '95*, pages 1874–1879, Sevilla, España, 1995.
- [12] M. Aredes, J. Häfner, and K. Heumann. Three-phase four-wire shunt active filter control strategies. *IEEE Trans. on Pow. Electronics*, 12:311–317, 1997.
- [13] M. Ucar, E. Ozdemir, and M. Kale. An analysis of three-phase four-wire active power filter for harmonic elimination reactive power compensation and load balancing under non-ideal mains voltage. In *Proc. IEEE Pow. Elec. Spec. Conf. (PESC)*, pages 3089–3094, Aachen, Germany, 2004.
- [14] P. Verdelho and G.D. Marques. Four-wire current-regulated PWM voltage converter. *IEEE Trans. on Ind. Appl.*, 45:761–770, 1998.
- [15] Vázquez, J.R. and P. Salmerón. Active power filter control using neural network technologies. *IEEE Proc. Elec. Power Applic.*, 150:139–145, 2003.
- [16] J.C. Montaño and P. Salmerón. Strategies of instantaneous compensation for three-phase four-wire circuits. *IEEE Trans. Power Delivery*, 2002.
- [17] R. Zhang, H. Prasad, D. Boroyevich, and F. Lee. Three-dimensional space vector modulation for four-leg voltage-source converters. *IEEE Trans. on Pow. Electronics*, 17:314–326, 2002.
- [18] M. Perales, M. Prats, R. Portillo, J. Mora, J. and León, and L. Franquelo. Three-dimensional space vector modulation in abc coordinates for four-leg voltage-source converters. *IEEE Power Elec. Letters*, 1:104–109, 2003.
- [19] J-H. Kim and S-K. Sul. A carrier-based PWM method for three-phase four-leg voltage source converter. *Proc. IEEE Pow. Elec. Spec. Conf. (PESC)*, 1:66–75, 2004.

-
- [20] A. Nava-Segura and G. Milo-Aguilar. A novel four-branches-inverter-based-active-filter for harmonic suppression and reactive compensation of an unbalanced three-phase four-wires electrical distribution system, feeding ac dc loads. *Proc. IEEE Pow. Elec. Spec. Conf. (PESC)*, pages 1155–1160, 2000.
- [21] E. Clarke. *Circuit analysis of A-C power*. John Wiley and Sons., New York, 1941.
- [22] G. Escobar, M. Stanković, and P. Mattavelli. An adaptive controller in stationary reference frame for d-statcom in unbalanced operation. *IEEE Trans. on Ind. Electr.*, 51:401–409, 2004.
- [23] R. Ortega, P.J. Loria, A. and Nicklasson, and H. Sira-Ramirez. *Passivity-based Control of Euler-Lagrange Systems*. Springer-Verlag, ISBN 1852330163, 1998.
- [24] H.K. Khalil. *Nonlinear systems*. Prentice Hall, 2nd edition, 1996. ISBN 0-13-228024-8.
- [25] P. Mattavelli. A closed-loop selective harmonic compensation for active filters. *IEEE Trans. on Ind. Appl.*, 37:81–89, 2001.
- [26] N. Nise. *Sistemas de control para ingeniería*. CECSA, ISBN 9702402549, 2004.
- [27] W.S. Levine. *The control handbook*. IEEE press., ISBN 0849385709, 1998.
- [28] B.A. Francis and W.M. Wolham. The internal model principle for linear multi-variable regulators. 2:170–195, 1975.
- [29] M. Mohan, T.M. Underland, and W.P. Robbins. *Power Electronics: Converters Applications and Design*. Addison-Wesley, ISBN 0471584088, 1995.
- [30] G. Escobar, A.A. Valdez, and Torres-Olguin R.E. A repetitive-based controller in stationary reference frame for d-statcom in unbalanced operation. *IEEE Int.Sympon Ind.Electronics. (ISIE)*, pages 1388–1393, 2006.
- [31] G. Escobar, A.A. Valdez, and Torres-Olguin R.E. Power factor correction with active filter using a repetitive controller. *IEEE Int.Sympon Ind.Electronics. (ISIE)*, pages 1394–1399, 2006.